WELDING OF CAST A359/SiC/10p METAL MATRIX COMPOSITES

A Thesis

by

MITUL ARVIND KOTHARI

Submitted to the Office of Graduate Studies of
Texas A&M University
in partial fulfillment of the requirements for the degree of

MASTER OF SCIENCE

August 2005

Major Subject: Mechanical Engineering

WELDING OF CAST A359/SiC/10p METAL MATRIX COMPOSITES

A Thesis

by

MITUL ARVIND KOTHARI

Submitted to the Office of Graduate Studies of
Texas A&M University
in partial fulfillment of the requirements for the degree of

MASTER OF SCIENCE

Approved by:

Chair of Committee,	Wayne NP Hung
Committee Members,	Richard Griffin
	Angie Hill Price
Department Head,	Dennis O'Neal

August 2005

Major Subject: Mechanical Engineering

ABSTRACT

Welding of Cast A359/SiC/10p Metal Matrix Composites. (August 2005)
Mitul Arvind Kothari, B.S., Mumbai University
Chair of Advisory Committee: Dr. Wayne NP Hung

Welding of metal matrix composites (MMCs) is an alternative to their mechanical joining, since they are difficult to machine. Published literature in fusion welding of similar composites shows metallurgical problems. This study investigates the weldability of A359/SiC/10p aluminum SiC MMC. Statistical experiments were performed to identify the significant variables and their effects on the hardness, tensile and bending strengths, ductility, and microstructure of the weld. Finite Element Analysis (FEA) was used to predict the preheat temperature field across the weld and the weld pool temperature.

Welding current, welding speed, and the preheat temperature (300-350°C) affected the weld quality significantly. It was seen that the fracture of the welded specimens was either in the base MMC or in the weld indicating a stronger interface between the weld and the base MMC. Oxides formation was controlled along the weld joint. Low heat inputs provided higher weld strengths and better weld integrity. It was found that the weld strengths were approximately 85% of the parent material strength. The weld region had higher extent of uniform mixing of base and filler metal when welded at low currents and high welding speeds. These adequate thermal conditions helped the SiC particles to stay in the central weld region**.** The interface reaction between the matrix and SiC particles was hindered due to controlled heat inputs and formation of harmful Al_4C_3 flakes was suppressed. The hardness values were found to be slightly higher in the base metal rich region. There was no significant loss in the hardness of the heat affected zone. The ductility of the weld was considerably increased to 6.0-7.0% due to the addition of Al-Si filler metal.

DEDICATION

I would like to dedicate my study to my parents, Mr. Arvind Kothari and Mrs. Nirmala Kothari, who made me the man I am today. They supported my decision of studying abroad and it took many efforts from them to make my dreams come true. They have been very loving and unselfish and were always there to provide me with the encouragement and support that I always required.

ACKNOWLEDGMENTS

I would like to express my deep thankfulness to my committee chair, Dr. Wayne NP Hung, for his dedication to his students. He had the time and passion to know exactly where I was heading during this entire study. He always offered me support in my efforts and new opportunities to explore. He has a vast expertise in composite materials and I am honored to have had the opportunity to work with him. I appreciate his serving as the committee chair in this study.

I would like to acknowledge my committee member, Dr. Angie Hill Price for helping me with her expertise in welding. She was always willing to share ideas and guide me throughout this study. She provided me with resources which I could explore for my research. She was also very kind in permitting me to use her metallographic equipment in her laboratory. I also wish to express my gratitude to Dr. Richard Griffin, for serving as my committee member. In the discussions that I had with him, he provided me with valuable information from his vast material science expertise. He showed interest in my work and would ask me thought-provoking questions which made me think to the next level.

I also thank Dr. Louis McDaniels for his design of experiment expertise. He was very kind in permitting me to attend his lectures on factorial experiments. Further, I thank Dr. Clint Bertrand who allowed me to use his material testing laboratory for testing my specimens. Mr. Frank Cervantez and Mr. John 'Butch' Macek at the Engineering Technology and Industrial Distribution Department, were always helpful in providing me with all the equipment and welding accessories.

I sincerely thank Mr. Mukul Agnihotri, my friend, who was very generous in helping me out with Finite Element Analysis of my study. Finally I would like to thank all my dear friends who were always there for me, to help me with my work. I will always cherish the laughter and the special moments that I shared with them.

TABLE OF CONTENTS

LIST OF FIGURES

FIGURE Page

FIGURE Page

LIST OF TABLES

NOMENCLATURE

AC	Alternating current
ACHF	Alternating current high frequency
DCEN	Direct current electrode negative
DCEP	Direct current electrode positive
DOE	Design of experiments
FSW	Friction stir welding
GMAW	Gas metal arc welding
GTAW	Gas tungsten arc welding
HAZ	Heat affected zone
HF	High frequency
MMC	Metal matrix composite
MMCs	Metal matrix composites
NDE	Non-destructive examination
SAW	Submerged arc welding
SMAW	Shielded metal arc welding
TMC	Testing, measurement, and control
UT	Ultrasonic testing
VHN	Vickers hardness number
VT	Visual testing

CHAPTER I

INTRODUCTION

Composite materials have been one of the major areas of scientific and applied research for many decades; however, only in the past decade they have been viewed and applied as engineering materials. Today we have significant progress and advances in our understanding of these materials and their metallurgical behavior. The greatest advantage is in the fact that we can inherit properties of both, the metal matrix and the reinforcements, providing a material with properties which can meet specific and challenging requirements in many applications. There is a wide spectrum of the types of metal matrix composite (MMC), each with a specific property profile. The conventional format of citing a MMC is matrix/reinforcement/volume % and type of reinforcement. The composite material under consideration, which is cast 359 aluminum silicon alloy reinforced with 10 volume % of SiC particulates, is cited as A359/SiC/10p. These metal matrix composites (MMCs) using aluminum as the matrix such as A359 with SiC particles reinforced in it (A359/SiCp), have found vast applications in automotive, aerospace, and marine and other allied fields, which have aggressive environments. They are also used in medical applications such as for electronic detectors in magnetic resonance imaging (MRI) systems and in computerized tomography (CT) scanners. Further, they are very suitable for heat dissipation applications in electronic devices and assemblies due to their high thermal conductivity. We are thus currently at a stage where A359/SiCp MMCs can be further explored according to our needs.

Despite their potential applications, limited joining and machining processes have hindered their wide market usage. Joining methods such as mechanical bonding of these materials result in excessive tool wear and are relatively expensive.

This thesis follows the style and format of Materials Science and Engineering A.

Further, non conventional welding methods such as friction stir welding, though very effective are also expensive. Conventional fusion arc welding processes provide a better alternative for joining them. Most of them are economical, flexible and have been in the industry for many decades.

Welded components and structures are widely used in almost all industries. Present day engineering industry relies heavily on welded components and structures. Therefore, weld integrity becomes important for adequate and reliable performance of components, structures, and plants. Weld integrity is dependent on the base material, specifications, and welding processes. With the ever-increasing sophistication of processes, materials, and specifications, one must have a broad, comprehensive knowledge of the metallurgy and welding processes.

Fusion welding of MMCs has been found difficult because of different properties of the base matrix and the particulate reinforcements. Novelty and relative complexity of composites add unwanted complications to an already challenging field. All these provide hindrances in effective and reliable weld joints in composites. For instance, concerns such as solidification defects due to difference in the densities of the aluminum matrix and the reinforcement, chemical reactions when subjected to prolong heating during welding, and lastly, precise and accurate weld preparation to avoid tearout or cracking have limited their applications. Further, the use of composite materials requires us to stay from the established processes and areas of practice that were relevant to more conventional engineering materials. Except for gas tungsten arc welding (GTAW) and gas metal arc welding (GMAW), all other conventional processes of welding have been found ineffective [1]; however, the effects of the welding variables in the above processes on the weld properties are known to a limited extent. It is not known adequately how to improve their weld performance by appropriately modifying these welding parameters. Analysis of various welding parameters which affect properties of the completed weld will help to enhance their mechanical properties. It will also improve the structural integrity and also secondary materials properties such as stress corrosion resistance and fatigue strength.

At this stage, exploring welding of aluminum silicon carbide (Al-SiC) MMCs can serve as a motivation to further exploration of these MMCs. The parent metal, A359/SiC/10p was provided by Duralcan Composites. They have also manufactured them through permanent mold casting and other foundry processes, in addition to sand casting process. All these MMCs have been known for their excellent high strength-to-weight ratio, high abrasive resistance, and excellent wear resistant properties.

It was decided to determine the weldability of the above MMC in this study in the light of the welding concerns previously mentioned. Determining the weldability of the MMC in this study refers to analyzing the microstructure of the welded MMC and evaluating their properties as a function of the input variables. This necessarily did not mean to make a full penetration butt joint; it rather was intended to achieve sound welds with minimum weld defects, with the joint geometry selected in this study. Also, it was found necessary to study, set, and perceive optimal conditions for welding the MMC to enhance their strength and microstructural integrity. To begin with, GTAW was selected for welding this MMC. Since it was known from literature review that amongst the fusion arc welding processes, GTAW is the preferred process; all the experiments were performed with GTAW. All the welding relating variables were listed and based on the results of some preliminary tests, they were screened and eventually welding current and welding speed were selected as the input variables for the final design of experiments. This decision was also based on financial considerations. Design of experiments is a tool which helps to analyze and predict the effect of the influential parameters on the response variables in interest. The study was focused on the resulting strength of the welded MMC, its ductility, and its microstructural integrity. Tensile and bend tests gave a very good indication of the weld joint characteristics along with its ductility. Microstructural analysis along with microhardness tests helped to correlate the data obtained from the above destructive tests. Finally, Finite Element Analysis (FEA) was used to predict the preheat and the weld pool temperature.

CHAPTER II

OBJECTIVES AND SCOPE

The objectives of this study are divided as follows:

1. Studying the weldability of A359/SiC MMC

The main objective of the research was to determine the weldability of the cast MMC, A359/SiC. Further, to enhance the weld quality and performance, optimization of the welding parameters for the MMC was required. It was aimed to achieve high strength welds. One of the objectives also was to have high ductility weldments without significant loss in their strengths.

2. Investigating the effects of the welding characteristics on the parent microstructure

It was intended that the welding process should have minimum impact on the MMC. The welded MMC and the parent MMC should have substantial amount of similarities at the microstructural level. It was of prime importance to avoid any interface reaction between the constituents of the MMC. Only then one can obtain uniform results and consistent performance when a welded MMC is put in service. Knowledge of welding characteristics thus was necessary to obtain best results in terms of weld quality and improved weld performance.

It was the aim of this study to investigate the consequences on the weldment by minimizing at every point the influence of these factors on potential failure and on the avoidance of defects. Through this study an attempt was made to analyze the effect of the welding input characteristics on the primary properties of the weld joint and on the MMC as a whole when in use for a particular application. With the realization of the fact that weld is the weakest link, the objective of the project dwelled in the fact that more and more emphasis is required for fabricating high quality welded MMCs. It is hoped

that this research will go some way towards giving an appreciation of the problems of welding the Al-SiC MMCs and guidance on how these problems may be overcome.

The scope of the project lay in the following:

1. Determining significant welding variables

Effects of welding variables on the MMC are to be studied. It is proposed to determine their influence on the weld properties through design of experiments (DOE). Factorial experiments are to be conducted to screen the non-significant variables and to choose comparatively significant welding variables.

2. Welding, testing, and evaluation methods

It is proposed to weld these MMCs by a mechanized GTAW process. The testing and evaluation methods to be used are destructive tests such as tensile, bending and impact tests, and optical microscopy for microstructural analysis. The welded MMCs are to be further evaluated for determining the variation of microhardness across the weld. These evaluation methods are expected to be sufficient to determine the impact of the influential welding variables on the weld properties.

3. Finite element analysis

With regard to finite element analysis, an attempt is to be made to simulate the thermal aspects of the welding process. The aim is to simulate the welding process and determine the preheat temperature field across the MMC and the weld pool temperature subsequently. The findings then are to be compared with experimentally measured values.

CHAPTER III

LITERATURE REVIEW

Review of the published research work in the welding of MMCs revealed that welding of the MMC in question has been very limited. Duralcan Composites, who manufacture and provided us with these MMCs, too have provided little information on the effects of the influential welding variables on the weld quality. Previous studies have been undertaken in this particular field, but on other types of MMCs, barring this. In this section, some fundamentals about relevant topics on metal matrix composites and welding terminologies are discussed. Also, relevant information on the composite, its welding, testing, and metallurgical analysis from the previous related studies has been included.

III.1. Metal matrix composites

A MMC can be described as a material which is made up of a continuous metallic phase (the matrix) into which a second phase (or phases) has been artificially introduced. Initially, mechanical properties of light alloys were improved by the reinforcement of fibers, mainly ceramics. The microstructures of continuous fiber are equivalent to those in polymer matrix composites. Early MMCs had their application confined to military and aerospace applications; their extensive usage was hindered due to their high production costs, limited production methods, and restricted product forms.

The properties of MMCs are comparatively superior as compared to the unreinforced alloys. Some of the typical important properties of particle reinforced MMCs are compared with the conventional alloys, as listed in Table 1 [2,3]. The properties of particle reinforced metals or with short fibers (whiskers) are modest compared to the continuous fiber reinforced MMCs; however, these discontinuous reinforced materials are less expensive to fabricate and have flexible production

techniques. Thus, they are cost effective and can be exploited more as compared to other types of composites, of course, depending on the applications where they are to be used.

Table 1

Comparison between properties of a conventional Al alloy and a MMC with the same Al alloy as the matrix [2,3]

Material	**Tensile Strength (MPa)**	**Abrasive Resistance (Volume loss, mm^3)**	**Wear Resistance (Volume loss, mm^3)**
A356 – T6	228	0.575	0.18
A359/SiC/20p –T6	340	0.202	0.023

The factors influencing the type and form of reinforcement used are the material properties desired, ease of processing, and part fabrication. In early stages of developments, only a limited range of reinforcements could be used. The stability between the components and the differences in their thermal properties such as coefficient of thermal expansion and coefficient of thermal conductivity are the limiting factors in the compatibility of the two materials used to make the composite. A good bond only can be formed by proper and adequate interaction between the reinforcement and the matrix. Inadequate interaction results in lack of proper bonding, whereas excessive interaction leads to the loss of the properties desired and inferior performance of the MMC.

In some cases, the reinforcement requires coating to avoid interaction between the constituents of the composites or to improve the reinforcement wettability. For instance, the wettability of mica has been shown to be improved by the addition of magnesium to the aluminum melt. Similarly, carbon fibers are coated with a titanium boride layer to enhance wettability [4].

As mentioned earlier, the recent focus is on particulate reinforcements MMCs due to their low cost of fabrication. The major reinforcements used in aluminum MMCs are silicon carbide, boron, graphite, and alumina. Most of the current research work is focused on SiC and Al_2O_3 reinforced aluminum MMCs, the main reason being low cost and high availability.

The SiC/Al interface reaction proceeds according to the equation:

$$3SiC + 4Al \rightleftharpoons Al_4C_3 + 3Si \qquad (1)$$

The thermal conditions for this reaction depend on the composition of the MMC and its processing method. As the reaction progresses, the activity of silicon in liquid aluminum increases and the reaction tends to saturate. The presence of free silicon in an aluminum alloy has been shown to inhibit the formation of Al_4C_3 [4]. Temperature control is extremely important during the fabrication process. If the melt temperature of SiC/Al composite materials rises above a critical value, Al_4C_3 is formed, increasing the viscosity of the molten material, which can result in severe loss of corrosion resistance and degradation of mechanical properties in the cast composite; excessive formation of Al_4C_3 renders the melt unsuitable for casting [4].

The material in consideration was cast A359/SiC/10p, provided by Duralcan. It has 8.50-9.50% Si by weight. It is known that molten aluminum does not wet silicon carbide readily, which is one of the major concerns which needs to be overcome to prevent silicon carbide particles being displaced from molten aluminum and to ensure SiC/Al bonding [4]. In addition, as mentioned, heating above a critical temperature can lead to the undesirable formation of Al_4C_3 flakes. Duralcan patented melt stirring, a method of satisfying these requirements and producing high quality composites, in 1987. SiC particulates are added to Al-Si casting alloys where Si in the alloy inhibits the formation of Al_4C_3. Apart from Duralcan, COSPRAY patented a spray deposition route for manufacturing MMCs. The process yields material with a uniform distribution of

particles in a 95-98% dense aluminum matrix. The rapid solidification inherent in the process ensures minimal reaction between reinforcing material and the matrix.

III.2. Welding

Welding can be described as the joining of two pieces by a coalescence of the areas in contact with each other. This can be achieved by different means. Welding processes could be autogenous *welding,* involving only the fusion of the base metals. The other class of welding processes involves the use of a filler metal which is continuously added and melted in the joint. The weld metal would be then comprised of the melted base metal along with the filler metal.

The welding techniques can be classified in general as fusion welding and solid state welding. Fusion welding, as the name suggests, welds the components by melting them. On the other hand, in solid state welding processes, the joining of two parts is done by bringing them together under pressure, associated with or without heat input, to form a metallic bond. Gas tungsten arc welding (GTAW), a type of fusion welding process, was used in this study.

III.2.1. GTAW

GTAW uses a non-consumable tungsten electrode and an inert gas to protect the weld pool, electrode, and arc column. One of the advantages of GTAW is that the arc remains stable even at very low welding currents.

The bulk of the heat is produced at the positive terminal. If the tungsten electrode is connected to the positive pole using DC current i.e. DCEP (Direct current electrode positive), then it melts because of overheating. Further, cleaning action due to the breaking of the oxide film on the specimen occurs during DCEP. GTAW with DCEN (Direct current electrode negative) leads to efficient penetration during welding. Manual GTAW of aluminum is performed with AC. In AC type current, the oxide film removal

takes place on the electrode positive half cycle and electrode cooling and weld bead penetration occurs on the electrode negative half cycle. After every half cycle, the arc is extinguished and reignited [5].

Aluminum, being a poor emitter of electrons, presents more difficulty in reigniting the arc on the positive half cycle. If there is any delay in the reignition, then the current ceases to flow on the positive half cycle. This results in an unstable arc and the cleaning action is lost with a direct current component produced in the secondary circuit of the power source, leading to overheating of the transformer. This is prevented in modern equipment by inserting blocking condensers in the power source circuit.

Typically, the gas for AC-GTAW welding of aluminum is argon; however, helium and argon-helium mixtures may also be used. Argon gives a shallow penetration weld bead, but will leave the weld bright with a silvery appearance. Argon facilitates easy arc ignition with higher stability. Helium, because of its higher ionization potential, increases arc voltage, and has the effect of constricting the arc and increasing arc stability. Adding argon to helium significantly enhances the arc stability [6]. Travel speeds and penetration will be less than with pure helium but greater than with pure argon. Normally, 25% helium with argon is preferred [7].

Electrodes used are typically tungsten or tungsten alloyed with thoria (ThO_2) or zirconia (ZrO_2). These compounds improve the arc stability characteristics and higher service life. Recently, rare earth elements such as cesium, cerium, or lanthanum have claimed to improve the electrode life and have reduced the risks arising from radiation during the grinding of thoria containing electrodes [6].

The electrode used should not protrude from the nozzle by more than about 6 mm; although it may be extended to 10 mm if a gas lens is fitted to the torch. The hemispherical shape of the electrode tip should be maintained to achieve a stable arc.

Weld termination is important if defects such as craters, piping, and cracks in the finished weld pool. Reducing welding current gradually and to reduce the arc length as the arc fades away are important.

III.2.2. Defects in aluminum welds

Some common defects encountered in aluminum welds are also known to be found in Al MMC welds. Some features and defects that may contribute to the loss of properties as compared with the parent aluminum metal are listed below:

1. Porosity

Porosity arises from the gas dissolved in the molten weld metal, which become trapped during solidification, forming bubbles in the solidified weld metal. Hydrogen has low solubility in the solid but high solubility in molten aluminum, which is a major problem and results in the above defect. Increasing the heat input increases the weld pool temperature and enhances the rate of absorption of hydrogen in the molten weld metal; however, higher heat input can reduce porosity since in that case the rate of gas evolution from the weld exceeds the rate of absorption, slowing the rate at which the weld freezes and allows the hydrogen to escape out of the weld. Of the conventional fusion methods, GTAW has lower levels of porosity than GMAW due to less hydrogen contamination of the filler wire [6].

2. Oxides

Oxide film removal is needed to reduce the risk of porosity. It is also necessary to avoid welding defects such as lack of fusion and oxide film entrapment. Aluminum oxide forms very rapidly, and has a higher melting temperature (2060°C) as compared to the melting temperature of pure aluminum metal (660°C). Increasing the temperature of aluminum above its melting temperature will result in a layer of oxide, surrounding the molten aluminum pool. This oxide layer needs to be removed to prevent high risks of early service failures. In GTAW, AC is used where oxide film removal takes place on

the positive half cycle and tungsten electrode cooling on the negative half cycle. Proper inert gas is also required for adequate shielding of the weld pool and the arc column [6].

3. Hot cracking

The basic mechanism behind hot cracking is high temperature cracking mechanism and is a function of how metal alloy systems solidify. It is caused due to difference in the melting points of the different alloying elements added to the pure metal. In the aluminum alloys, the alloying elements form a range of eutectics with freezing points substantially lower than the bulk metal. Generally aluminum alloys are susceptible to some degree of cracking.

A term important in weldment terminology, hot short range, is the range of composition within which the alloy has a high risk of hot cracking and it should be avoided. To eliminate hot cracking, one can control the composition of the weld pool by adding filler metal to produce an alloy that is not in the hot short range. Adding a filler metal with a melting point close to that of the base metal reduces hot cracking. It was found that addition of filler metal while welding thin plates of dissimilar aluminum alloys in the range of 1.5 and 3 mm prevented hot cracking [8]. Using the highest welding speed reduces the time the weld is within the hot short temperature range. It also reduces the size of the heat affected zone (HAZ) and consequently the shrinkage stresses cross the joint. Small weld beads generally have better properties than large weld beads and a lower susceptibility to hot cracking, since fast solidification rates will give a finer grain size and better mechanical properties than slow solidification rates [6].

4. Loss of strength in HAZ

The heat input during welding leads to the formation of three distinct areas in the weld joint: the weld metal, the HAZ in the base metal, and the unaffected base metal. Since the HAZ experiences one or more cycles of heating and cooling, the properties of

the weldment are different from those of the unaffected base metal. Only when the alloy is in the as-cast or annealed condition, the properties of the HAZ match those with the base metal. It has been known that heat input affects the weld quality and should be minimized to narrow the HAZ. Also, the HAZ impact strength increases when the specimen are welded in the horizontal position, while its hardness decreases [9].

Cold-worked alloys experience a loss of strength due to recrystallisation in the HAZ. Recrystallisation is found to start at temperatures of approximately 200°C in the HAZ, and increases further with full annealing at 300°C in any cold worked 1000 series of aluminum alloys [6]. This results in significant loss of strength in the HAZ. One of the research works in the field of welding dissimilar aluminum alloys also revealed that the lowest hardness values across the weld were obtained in the HAZ of the material AA5754-H32, while welding AA5083-O and AA5754-H32. Further, there was no significant loss of strength in the annealed AA5083-O material [8].

Another important aspect one needs to focus on is weld preparation and its design. The convenience with which a weld can be made depends on the joint design and there are some crucial factors for weld design one should keep in mind. Some of the important and relevant factors are welding speed, welding current, and welding position. They are discussed below.

a. Welding speed

Welding speed is defined as the linear rate at which the welding arc moves along the weld joint. Aluminum is welded generally at high speeds to avoid abrupt and sudden changes of direction. It is a very important parameter because it controls the actual welding time and the total heat input in the specimen. A proper estimate of the welding speed is required to attain high weld quality. Excessive welding speeds may cause porosity, undercut, and arc blow. With slow welding speeds, the penetration decreases with the weld bead getting wider; however, with increasing plate thickness, the welding speed should be reduced to facilitate good welds if the current is kept constant [8].

b. Welding current

Welding current is one of the most influential parameters in welding. The melting rate is directly proportional to the amount of heat energy supplied. It decides the extent of electrode melting, deposition rate, the amount of base metal melting, and the depth of penetration [7]. Increased welding current leads to weld induced distortions, while low currents lead to lack of fusion and penetration. Further, increasing heat input leads to wider HAZ. Also, with increase in heat input, the hardness in the HAZ decreases due to slow cooling rates leading to grain growth [9]. One therefore, should keep the current within recommended limits; however, it is found that the arc current needs to be increased for metals with higher thermal conductivity, such as for aluminum [8]. This is simply due to the fact that these metals lose heat faster than other metals with low thermal conductivity, and requires relatively higher heat inputs for better joint fusion.

c. Welding position

Generally, flat or downhand position is preferred for all welding processes. Flat position welding generally ensures good quality weldment with sufficient metal deposition rates. The weld pool is larger in this position with slow cooling rates, allowing the gases to evolve out of the pool and reducing porosity [7]. It is also seen that in the flat position, high heat input forms a wider HAZ at the weld corners, as compared to horizontal position welding [9]. For fillet welds in the horizontal-vertical position, the electrodes are inclined at 50°- 80° in the direction of travel and 40°- 50° to the flat plate. In that case, the force of gravity tends the weld pool to sag, making it difficult to obtain the desirable results [7]; however, some specific components and processes require positions other than flat position during welding.

Testing, measurement, and control (TMC) of welds deals with the design, fabrication, and quality assurance practices of welding. Testing of welds refers to the use

of destructive as well as non-destructive methods to evaluate weld quality [10]. Measurement of welds refers to the measurement of different welding variables that influence the quality of a weld joint. The parameters could be bevel angle, dimensions, welding current, heat input, etc. Control of welds relate to the steps that are taken from the recommended norms so that a welded joint meets the required design needs.

With regards to testing, destructive testing techniques are used to compare the weld properties with the base metal mechanical properties. In a destructive test technique, the welded specimen is bent, twisted, or pulled apart to check defects and mechanical properties. Destructive testing makes a product unusable. Destructive tests have been used for routine inspection with the assumption that results derived from such tests are typical of the complete lot from which the test samples were selected. The following are some of the destructive tests normally applied in practice.

Bend tests are applied for defining internal weld properties. These types of tests are made in a fixture to bend the material into a U form over a defined radius, which depends on the thickness and strength of the specimen. After bending, the outer face of the U is detected for cracks and other defects by as specified by welding standards. Fig. 1 shows a schematic representation of the different type of bend tests [11]. Standard guided bending tests, ASME Sec IX QW-462.3 (b), are generally used for qualifying welds.

Tensile tests are used to determine the ultimate strength of the welded joint i.e. the point at which the weld fails in tension, yield strength of the joint i.e. when the weld yields or stretches under tension and lastly elongation which determines the amount of stretch that occurs during the tensile test (Fig. 2) [12]. The dimensions of the specimen not specified in the figure depend on the length of the specimen and can be found in the standard transverse tensile test, ASTM E 8M.

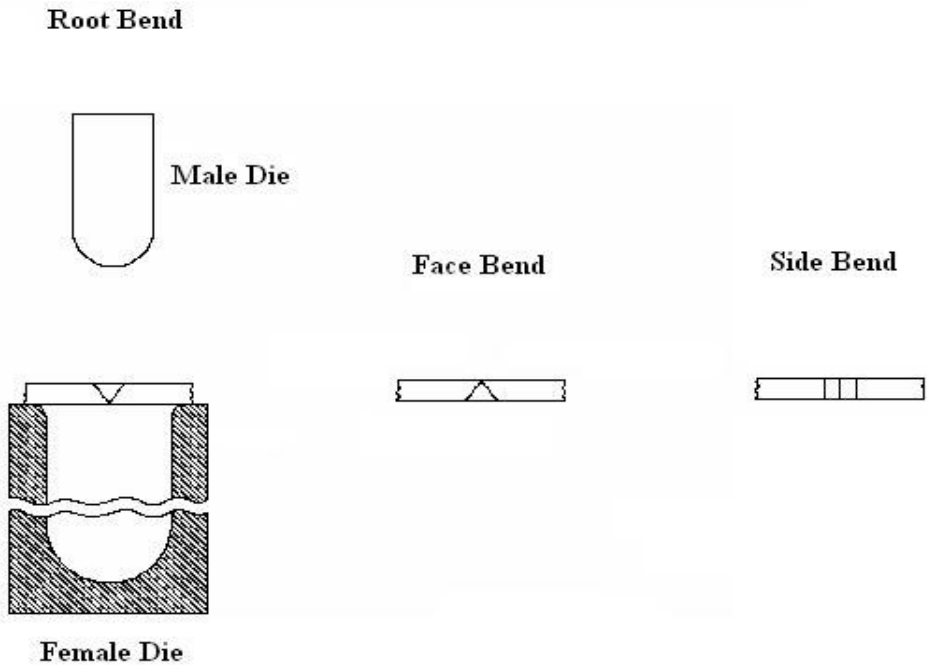

Fig. 1. Bend tests [11].

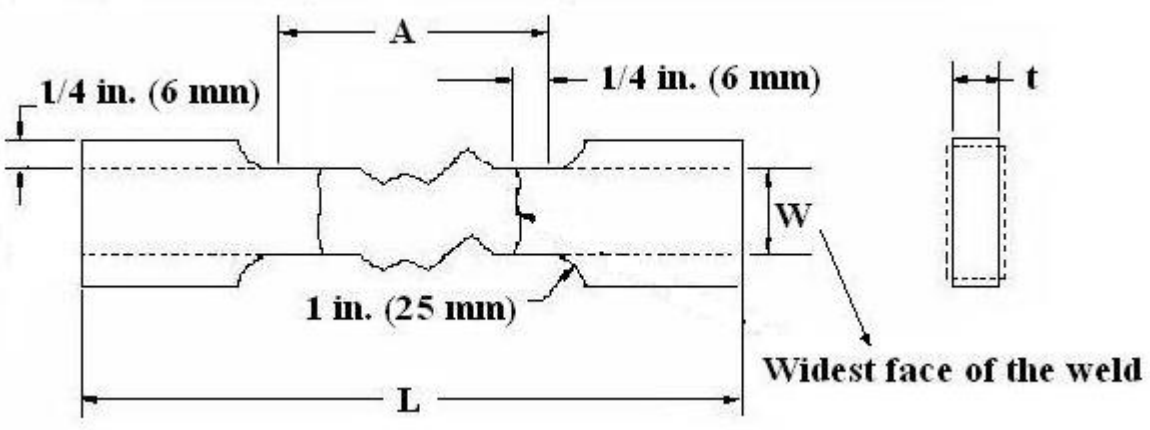

Fig. 2. Standard tensile test specimen [12].

III.3. Welding of metal matrix composites

Along with joining of homogenous materials, the vast joining technology should provide a variety of processes suitable for manufacturing high integrity joints with optimum mechanical properties and ease of inspection for composite materials and MMCs; however, there are inherent problems peculiar to MMCs during their joining.

Following are some of the potential problems encountered during joining of MMCs.

III.3.1. Solidification defects

Since most nonmetallic reinforcements have different densities from the metal matrix, this can lead to pronounced particle segregation effects when the matrix is in the molten state [13]. Below a certain critical solidification temperature, reinforcements can be pushed ahead of the solidification front, resulting in non-uniformity of the reinforcement in the weld region. Fig. 3 illustrates a GMA welded Duralcan W6A.20A-8511 torque transfer tube and 6061-T6 aluminum yoke. It is seen that the composite is diluted by the filler metal with non-uniform distribution of the reinforcement particles in the weld region.

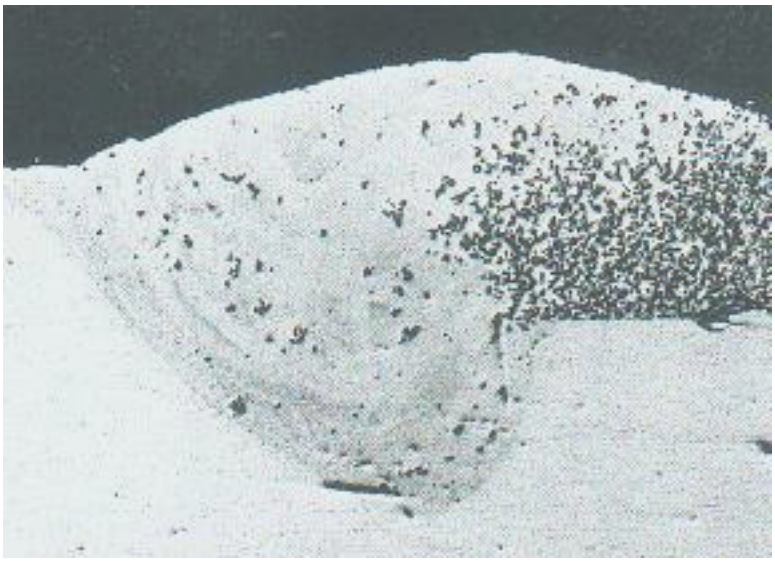

Fig. 3. GMA-welded Duralcan W6A.20A-8511 torque transfer tube and 6061-T6 aluminum yoke [2].

Under the molten state, composite metal weld pool has higher viscosity than the reinforced metal matrix and does not flow well. High viscosity also leads to a lower heat transfer by convection mechanism in the weld pool, which can affect the resulting microstructures and the stress distributions in the MMCs. The fluidity of the weld pool decreases due to the presence of the SiC reinforced particles. This can lead to increased porosity in the weld metal, as low fluidity may not be sufficient to ensure the filling of the entire weld pool region. Solidification problems may result in dissolution of the reinforcements and non uniform packing density of the reinforcement across the weld region [1].

III.3.2. Chemical reactions

One major difficulty with most of the fusion welding processes for MMCs is that prolonged contact between a molten metal matrix and particulate reinforcement can lead

to undesirable chemical reactions [13]. For example, liquid aluminum will react with SiC reinforcement to precipitate aluminum carbide (Al_4C_3) and also increase the silicon content upon cooling down the molten metal matrix, according to the interface reaction (1). These plate-like Al_4C_3 particles embrittle the structure. Studies on the interface reactions on the fracture mechanisms of Al MMCs welded with GTAW [14,15] revealed that the proportion of interfacial failure increased in the weld metal due to the formation of Al_4C_3. They reduced the strength of the interface bonding. Also, it was seen that Si, released during the above chemical reaction, further embrittle the weld metal. They also found that formation of intermetallic compounds (Si and Al-Fe) led to further embrittlement of the weld metal. They found that the tensile strength of the welded specimens was below 50% of the base material properties.

Previous works on welding of 6061 Al reinforced with 10% volume fraction of SiC particles revealed that GTAW tends to produce more Al_4C_3 platelets than pulsed-GTAW [16]. Fig. 4 shows the microstructure of the above MMC when welded with GTAW, clearly showing the Al_4C_3 platelets; however, they found that the addition of Al-Si filler metal helped to decrease the thermodynamic driving force of the above reaction, avoiding the interface reaction. Moreover, Al-Si increased the fluidity of the weld pool and the tensile strength was found to be higher than as compared to the welds added with other filler metal material. Addition of Al-Si also reduced the hot crack sensitivity of the weld, once again due to increased fluidity of the molten weld pool.

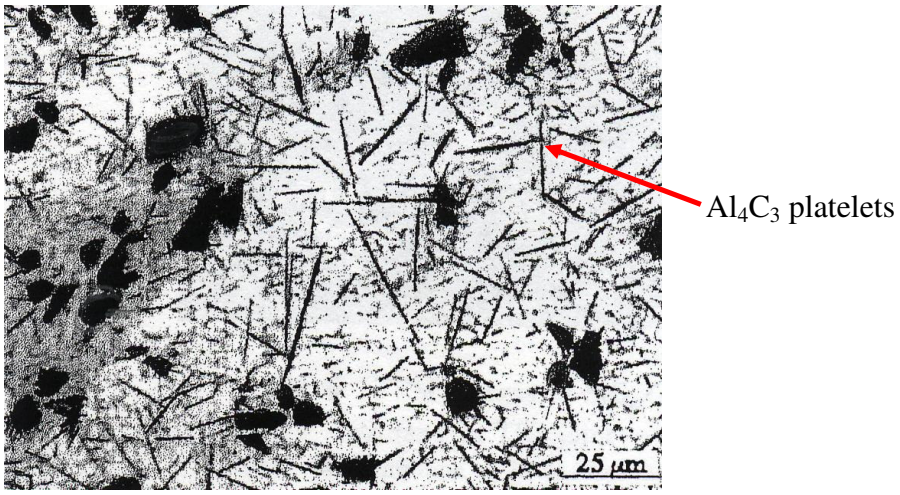

Fig. 4. Microstructure of GTAW joint on AA6061/SiC/10p [16].

Research work on CO_2 laser welding of A356/SiC with different amounts of volume fractions of SiC particles has been done [17]. The researchers calculated the thermal fields in the weld region and found the critical temperature conditions for aluminum carbide formation. They also concluded that weld cooling rate was a very important factor for controlling aluminum carbide formation. They determined the critical temperature required for Al_4C_3 formation as 827°C and the critical cooling rate as 12000 K/sec by formulating an analytical code and comparing those results with the experimental values. Cooling rates above the critical cooling rate tend to decrease the extent of the interface reaction. Similarly, a study conducted on fusion welding of Al-SiC MMCs predicted the critical temperature as 727°C for the formation of Al_4C_3 particles, based on thermodynamic considerations [1].

A study on the laser joining of A356/SiC with varying volume fractions of SiC particles was also conducted [18]. They too concluded that increasing energy densities increased the SiC particle dissolution and the formation of Al_4C_3 particles. Duty cycle had direct impact on the weld microstructure changes and found that intermediate duty

cycles provided optimum metallurgical changes. Fig. 5 illustrates a laser drilled A359/SiC/20p, which has a zone with Al_4C_3 needles in it, formed by the interface reaction [19]. Some instances of voids are also seen, which is typical in processed MMCs due to low fluidity of the molten MMC pool.

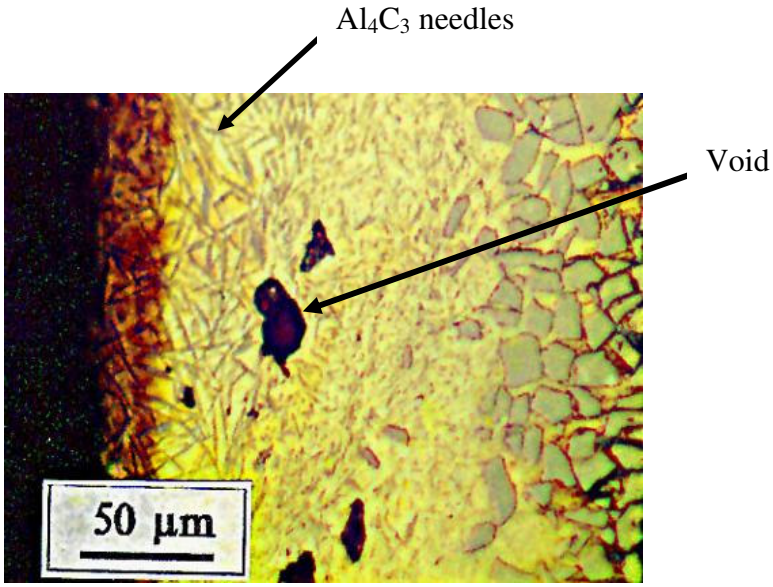

Fig. 5. Laser drilled A359/SiC/20p [19].

In the presence of moisture, metal carbides can decompose with the release of hydrocarbon gases and increase the joint susceptibility to corrosion cracking and joint strength degradation. Previous work [6] in the field of corrosion of welded Al MMCs revealed that pitting corrosion occurred in the HAZ, due to the formation of aluminum hydroxide according to the reaction:

$$Al_4C_3 + 12H_2O \longrightarrow 4Al(OH)_3 + 3CH_4 \qquad (2)$$

The chemical compatibility to the metal to reinforcement for a specific joining method thus is material and process specific.

III.3.3. Joint preparation

Because of the nonmetallic reinforcement, MMCs have low ductility, high surface-wear resistance, and high brittleness to machine, cut, or drill using high speed steel cutting tools and saw blades. In the preparation for an MMC joint prior to welding, the cutting and drilling parameters such as speed and force must be carefully controlled in order to avoid composite panel tearout or crack. During conventional machining processes such as turning, drilling, milling, etc., defects such as cracking of the matrix due to process-induced shearing stresses, fracture of reinforcing particles, or their drag out of the matrix in the direction of machining are encountered, as shown in Fig. 6 [20]. Many factors needs to be considered during machining of MMCs for weld preparation like matrix properties, hardness of the matrix, and reinforcing particle size and distribution (in the case of particle-reinforced MMCs).

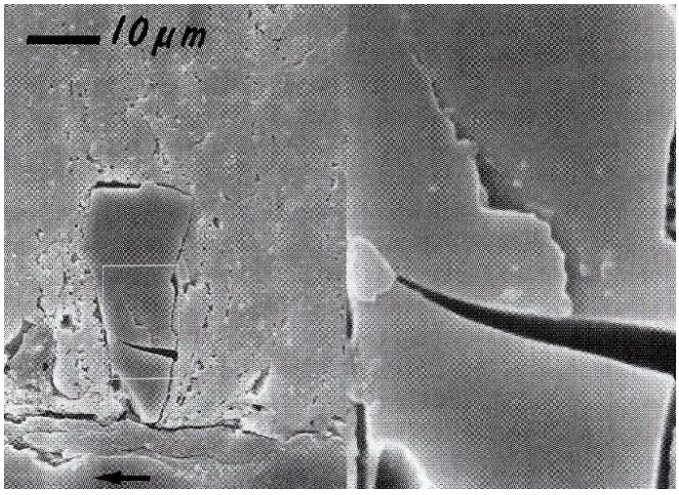

Fig. 6. Fracture of a SiC particle in Al-Li/SiC/20p due to machining [20].

In general, any joining technique for MMC depends on:

1. Volume fraction of reinforcement

The higher the reinforcement, the less likely it is for standard metal joining techniques to adapt. Discontinuous MMC are easier to join than MMCs with fibers, which are prone to matrix fiber debonding, delaminations, non-uniform density, and migration of fibers in the weld regions.

2. Metal matrix melting point

Longer time of exposure to heat input results to undesirable chemical reactions, and it accelerates as temperature increases. The higher the melting temperature, the less likely it is that most of the fusion techniques adapt.

3. Thermal energy management from the selected joining process

Excessive thermal input is undesirable. An automated joining process with less time and well-controlled thermal energy input is the best for joining MMCs.

CHAPTER IV

EXPERIMENTS

IV.1. Design of experiments

The primary intention of this study, as mentioned earlier, is to determine the weldability of cast A359/SiC/10p MMC. In an attempt to do so, it was required to find the right combinations of welding variables to weld it. It is also known that the chemical composition of the interface and the near-interface region plays an important role in the resultant mechanical properties of the MMCs. Typically, interfacial reactions between the reinforcement particulates and the matrix under high temperature conditions lead to the degradation of these properties. To maintain and achieve mechanical properties close to those of the base material, the welding conditions should provide the right environment for the adequate bonding between the base material and the filler alloy used. It thus was imperative to find the correct and optimized set of welding conditions for the MMC.

Design of experiments (DOE) was used as a tool to analyze the effects of these input welding variables. Two level factorial designs were used, implying that each factor had 2 'levels'. Levels are the values of the factors used in the experiments. So for instance, a high value and a low value of a factor such as 'welding speed' would be considered as its two levels. The levels can also be represented with a '–' (minus) and a '+' (plus) sign for low level and high level, respectively.

The test plan for the design of experiments was divided as follows:

1. Identifying possible welding variables for preliminary factorial tests
2. Preliminary factorial tests to screen out non-significant variables
3. Final factorial tests with significant variables
4. Optimizing significant variables for optimum results

IV.1.1. Identifying possible welding variables for preliminary factorial tests

Several input welding parameters were considered that are known to have significant impact on the weld quality. These variables are listed down in Table 2. Based on some experimental trial tests and published literature work [11,21], it was found that welding current, welding speed, and weld joint design had comparatively more influence on the nature of the weld pool and its properties. They were selected for the preliminary factorial tests. All these factors were considered to be independent of each other. The number of input parameters was limited to three, based on the limited number of the MMC blocks available for the experiments. The amount of time required for welding specimens and preparation for destructive testing and metallographic analysis also restricted the number of input factors for the experiments.

Table 2

Possible input parameters for preliminary factorial experimentation

Possible input parameters
Weld joint design
Welding speed
Welding current
Preheat temperature
Filler metal
Shielding gas

The response variables were then selected, i.e. the output variables which determine the quality of the weld. Impact strength was selected as one of the response variables so that it could give a quantitative depiction of the weld integrity. Microhardness test and microstructural analysis were considered to study the resulting weld microstructure and correlate it with data obtained from the Charpy V Impact test. The selected input and the response parameters are listed in the Fig. 7.

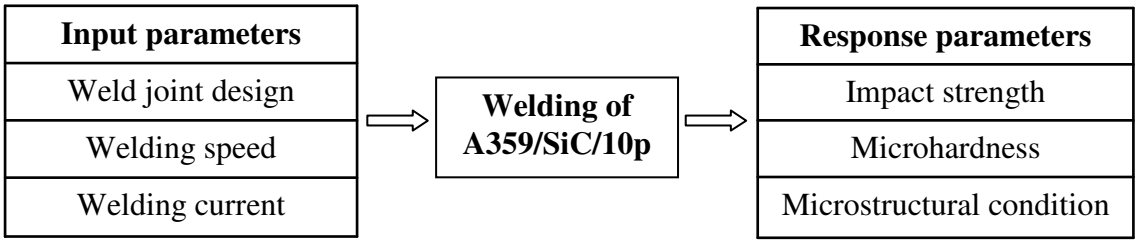

Fig. 7. Input and response parameters for preliminary factorial experimentation.

IV.1.2. Preliminary factorial tests to screen out non significant variables

As mentioned earlier, two level factorial designs were used. In this case, the levels of the input factors were selected within the range of recommended literature welding conditions [11,21]. The levels for the above input parameters are listed in Table 3.

Table 3

Levels for the input parameters

Input parameters	**Low level (-)**	**High level (+)**
Weld joint design	60° Double V	75° Double V
Welding speed	120 mm/min	250 mm/min
Welding current	90 amp, AC	110 amp, AC

As mentioned earlier, amongst the conventional fusion welding processes, GTAW is known to provide good results for welding Al MMCs and GTAW with AC type, balanced square wave was selected for all the experiments. Also, GTAW is economical and flexible.

Weld joint design refers to the kind of geometry and bevel edge preparation used for welding. A butt joint was selected, since it is the easiest to weld in flat position. It provides easy accessibility for welding. A double V butt joint design was selected to enable better penetration in the weld. The included angle has significant impact on the amount of penetration during welding. Further, it also reduces the amount of weld filler metal required in the weld as does the double V design.

Welding speed is one of the most important parameter in any type of welding, whether manual, semi-automatic, or automatic. It is the linear rate at which the welding arc travels along the weld line. It determines the thermal heat input per unit length and the amounts of filler metal deposited and the depth of penetration. It also determines the thermal conditions for the growth of the grains in the weld pool, which eventually determines the weld strength and load carrying capacity. The levels of the welding speed were selected within the range of recommended literature values [6,11] and within the limits of the dual side rack and pinion rail drive mechanism, as explained later used for semi-automatic welding.

Heat density, similarly is one of the most influencing parameters in welding. The melting rate is directly proportional to the amount of heat energy supplied. It decides the extent of electrode melting, deposition rate, the amount of base metal melting, and the depth of penetration. It also leads to weld induced distortions and determining the effect of this factor on the weld quality was inevitable. The levels of this factor were selected in accordance to the specimen size, experimental trials, and within the capacity of the GTAW machines available. The GTAW machine used was Lincoln Electric Square wave TIG 175 Pro. All the parameters other than the one mentioned above, were kept constant for all the experiments. Table 4 gives the listings of all such constants. Table 5 shows the combination of the parameters on which the preliminary factorial experiments were actually conducted.

Table 4

Description of constant parameters

Constant Parameters	**Value /Description**
Welding position	Flat
Preheat temperature	150°C
Electrode type and diameter	99.5% Tungsten, 2.54 mm (1/10”)
Arc length	4 mm
Shielding gas	Argon, 215 cm^3/sec (27.5 CFH)
Filler rod metal	R-A356.0, 4.76 mm (3/16”)

Table 5

Preliminary factorial experimentation

Test Run	Welding Current	Welding Speed	Weld joint design
1	-	-	+
2	+	+	+
3	-	+	-
4	+	+	-
5	+	-	+
6	-	-	-
7	-	+	+
8	+	-	-

IV.1.3. Final factorial tests with significant variables

Based on the results of the preliminary experiments as discussed later, the final factorial experiments were modified and only welding current and welding speed were used as the independent variables. It was realized that the amperage supplied by the GTAW machine available in the welding lab was not sufficient for complete penetration for the weld joint design initially selected. It was modified and then was used as a constant parameter rather than an independent response variable. Once again, this was based on the fact that the objective was to investigate the weldability of the MMC, rather than making a successful butt joint.

The values for the selected variables were still kept the same as those in the earlier experiments**.** The response variables were now changed to tensile strength and bending strength. Fig. 8 shows the design of the final factorial tests. It was found necessary to determine the location of failure in the welded specimen during destructive

testing to determine the weld integrity. Charpy Impact testing did not meet the objective of failing the specimens under slow loading and strain rates and was dropped. Ultimate tensile testing and four point bending test were selected, since the loading rate could be controlled and could be kept as low as required. Since 2 factors were now used in the experiments, it was a 2^2 factorial experiments leading to four test runs, as summarized in Table 6.

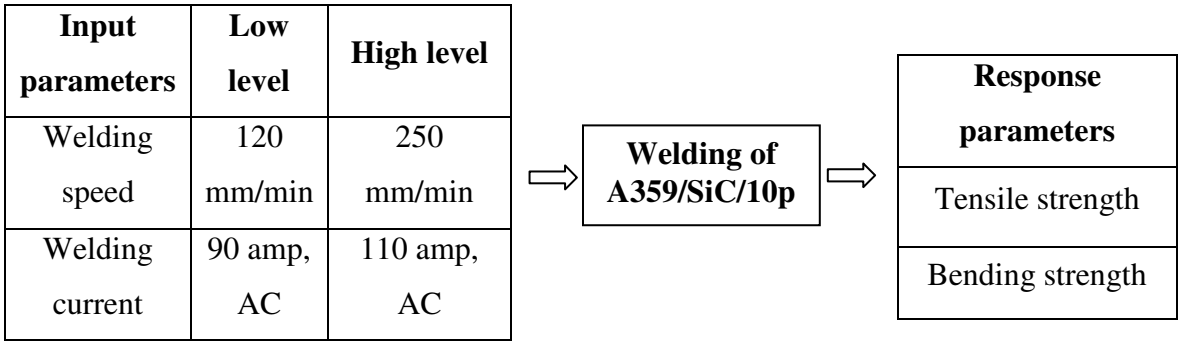

Fig. 8. Level of input parameters and response parameters selected for final factorial tests.

Table 6

Final factorial experimentation

Test Run	Welding Current	Welding Speed
1	+	-
2	+	+
3	-	-
4	-	+

IV.1.4. Optimizing significant variables for optimum results

All the results from the final factorial tests were analyzed using commercially available software, Design-Expert, DX6, version 6.0 for DOE. The results from the tensile tests were fed in the software and the results obtained were used for the analysis to determine the effect of the input variables. All the results with their analysis are explained in the chapter titled, "Results and Discussion". Based on these results and the interaction charts obtained from DOE, optimum levels for the welding variables were obtained to maximize the weld strengths. The optimized levels of the welding variables used in the experiments are listed in Table 7.

Table 7
Optimized level of the independent variables

Variable	**Optimized level**
Welding current	85 amp, AC
Welding speed	260 mm/min

IV.2. Materials

The chemical composition of the base MMC is listed in Table 8. The thermophysical properties of the parent MMC is listed in Table 9. Mechanical properties of this sand cast A359/SiC/10p MMC were not available from any published literature. They were tested by tensile and four point bending tests along with the testing of weld specimens, and their results are mentioned in the chapter titled "Results and Discussion".

The properties of permanent mold cast aluminum MMCs, however, are mentioned in Table 10.

Table 8

Composition of A359/SiC/10p [2]

Si	Fe	Cu	Mg	Ni	Ti	All other elements	Al
8.50-9.50	0.20 max	0.20 max	0.45-0.65	-	0.20 max	0.03 max-0.10 total	Rem. Rem.

Table 9

Thermophysical properties of A359/SiC/10p [2]

Material Property	**Value**
Density (Kg/m^3)	2710
Thermal conductivity (cal/cm-s-K)	0.450
Specific heat (cal/g-K)	0.235
Average coefficient of thermal expansion (10^{-6}/K)	24.8

Table 10

Mechanical properties of permanent mold cast Al-SiC MMCs - typical and minimum values [2]

Material	**Ultimate strength (MPa)**	**Yield Strength (MPa)**	**Elongation (%)**	**Elastic Modulus (GPa)**	**Rockwell Hardness, HRB**
A356 –T6	276 (min 255)	200	6.0	75.2	55
F3S.10S.T6	338 (min 310)	303 (min 283)	1.2	86.2	73
F3S.20S-T71	262	214	1.9	98.6	-
F3S.20S-O	221	165	2.8	98.6	-

The microstructure of the parent MMC has three distinct microconstituents. They are the aluminum matrix, the SiC particles, and the eutectic region of aluminum and silicon. The SiC particles were found to lie in the eutectic region. This is because, in cast MMCs, the SiC particles tend to aggregate in the eutectic region at the end of the solidification process. The distribution of SiC particles was found to be more or less uniform; however, instances of particle free zones and particle clustered zones were found. The Al/SiC interfaces had no interfacial reaction products. Fig. 9 shows a typical microstructure of the as-cast parent MMC. The aspect ratio of the particles was 1.5:1. The mean particle size was 12.8 ± 1.0 μm, with 94% population size greater than 5 μm and 3% population greater than 25 μm [19].

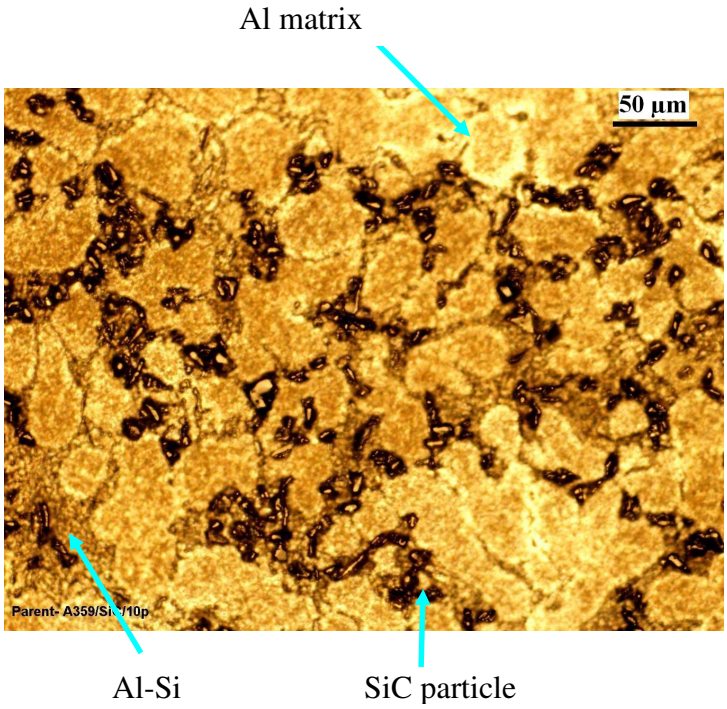

Fig. 9. Microstructure of the as-cast parent MMC.

The composition of the Al-Si filler metal used in all the experiments is listed in Table 11 [22]**.** It can be seen that the Si content in the filler metal and the base MMC were within 2%.

Table 11

Composition of Al-Si filler metal, R-A356.0 [22]

Si	Fe	Cu	Mg	Zn	Ti	Mn	All other elements	Al
6.50-7.50	0.20	0.20	0.25-0.45	0.10	0.20	0.10	0.15	Rem.

IV.3. Sample preparation

IV.3.1. Preliminary factorial tests

The weld joint design selected for the preliminary factorial tests is as shown in the Fig. 10. The specimens were milled to the dimensions shown. The milling cutters used for machining these specimens were standard high speed carbide tools and metal cutting oil-based lubricant was used during their machining. A double V butt joint was selected to facilitate better penetration, and at the same time, minimize the use of filler metal used.

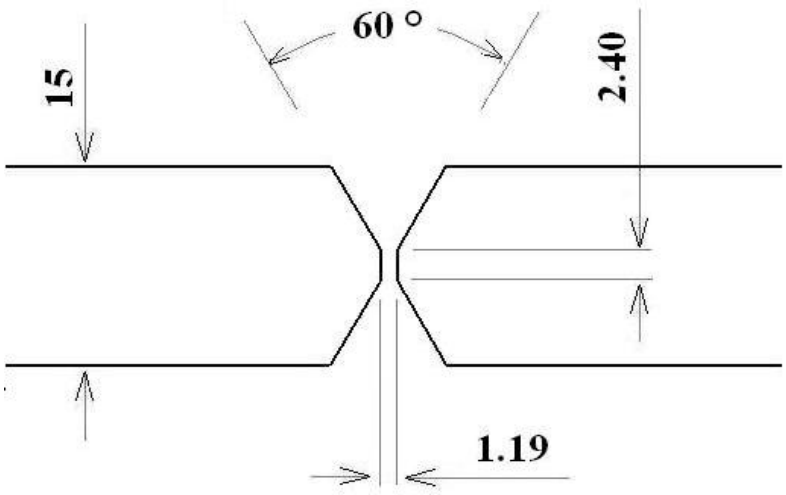

All dimensions are in mm

Fig. 10. Weld joint design for preliminary factorial tests.

IV.3.2. Final factorial and optimized tests

Instead of a double V butt joint design, a 90° single V design with 2.5 mm depth was milled as shown in Fig. 11 and welding was done along the groove as explained later. This V joint design was used since it was important to find the location of the failure during tensile and four point bending tests, rather than to join two MMC pieces through a butt joint. Further, it was intended to see if the interface reaction (1) occurs or not during welding process in the weld zone.

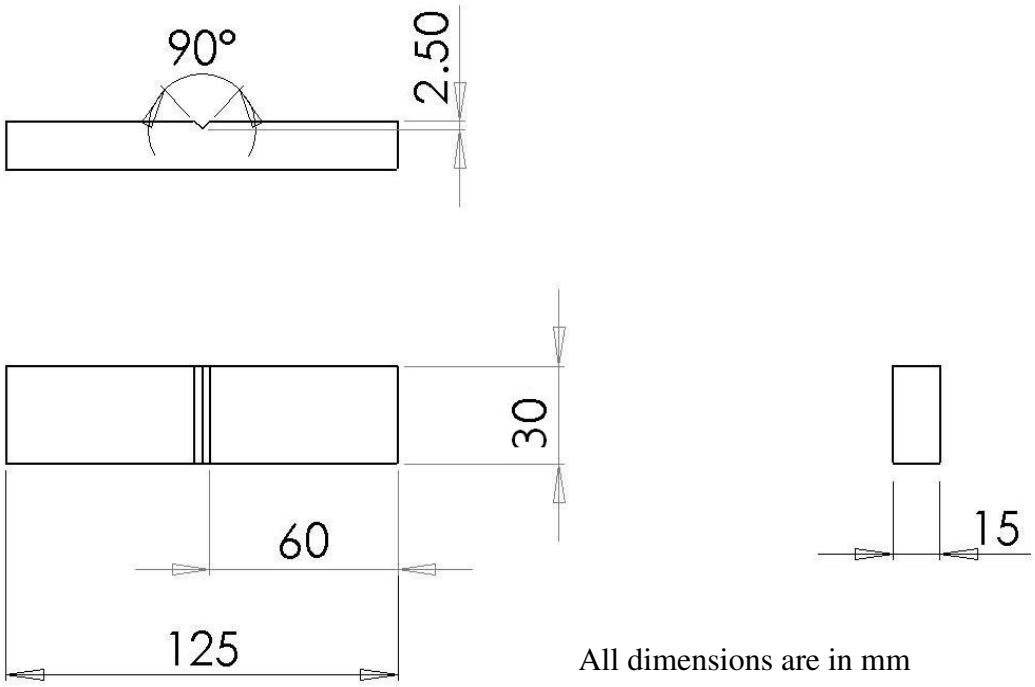

Fig. 11. Weld joint design for final factorial tests.

IV.4 Equipment and calibration

The following equipment was used for the experimental work and later for the testing of the specimens:

1. GTAW machine – Lincoln Electric Square wave TIG 175 Pro.
2. Dual side rack and pinion drive – Victor Mod 100
3. Universal Testing Machine (UTM) – United Calibration Corp. SFM 30
4. Mounting press – Buehler Simplimet 2
5. Vibrator Polisher – Buehler Vibromet 2
6. Optical microscope – Olympus STM6
7. Buehler Micromet 2 – Digital Microhardness Tester
8. DOE software – Design Expert version 6.0
9. Thermocouple data acquisition logger - Datapaq Reflowpaq 2000, Model RP0061

The UTM used was calibrated using known weights. The load cell calibrated was of 2000 lbs. capacity. The values obtained for the known forces were plotted and a polynomial line was curve-fitted line through these data points. The graph obtained is shown in Fig. 12. This polynomial line was used later for all future calculations. The values obtained from the destructive tests of the welded specimens were extrapolated on this polynomial line and the corresponding ideal force i.e. its true value was calculated; however, the 30000 lbs. load cell was not calibrated, since it was not possible to find high range forces.

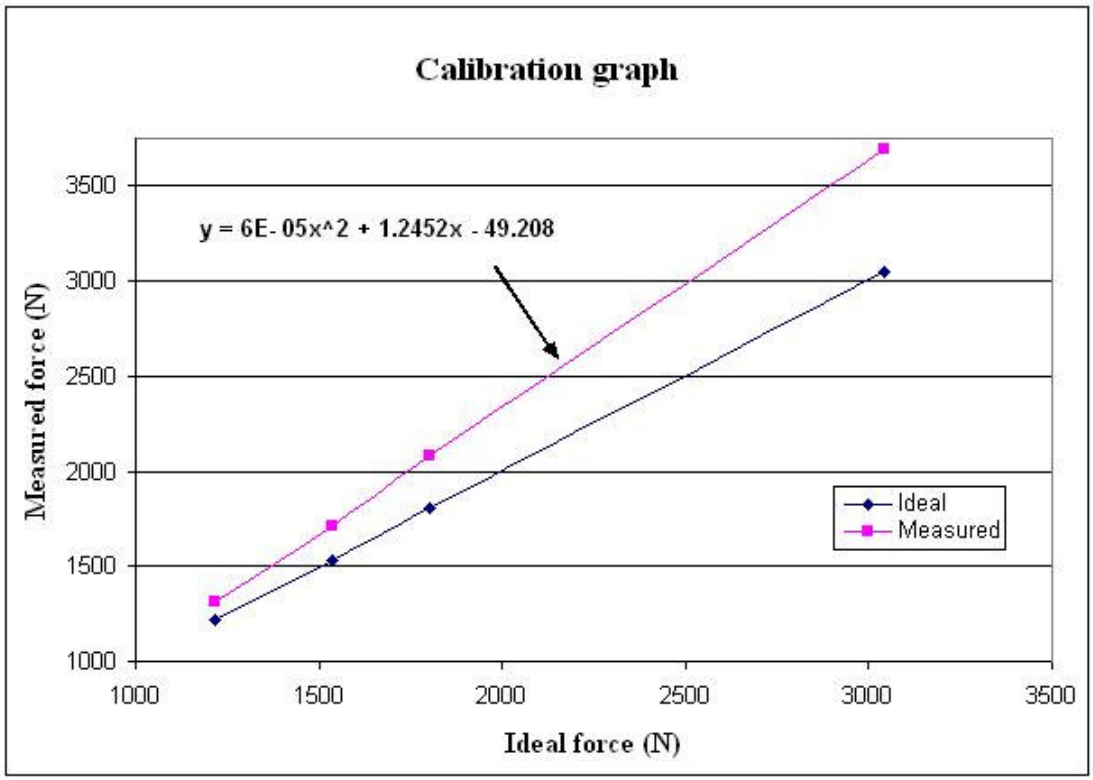

Fig. 12. Calibration of the Universal Testing Machine.

IV.5. Procedure

The entire experimental procedure was divided into:

1. Experimental set-up
2. Welding
3. Sample preparation for testing

IV.5.1. Experimental set-up

An experimental set-up was required to enable the mechanized GTAW process, so that consistent and accurate results could be achieved, minimizing human factors and their related errors. To achieve this, a dual side rack and pinion rail drive mechanism was used (Victor, Mod 100). The welding torch was attached to this drive at 15° to the vertical, away from the direction of welding. The rail drive had different calibrations on it, not suitable for the experiments. It was calibrated by performing trial runs i.e. in the forward and the backward direction. The average was then used for experiments. The time was measured with a stop watch for the rail drive to travel known distances and the actual velocities for different calibrations of the machine were calculated. The plot of the actual and calibrated values of the velocities is shown in Fig. 13. Further, leveling screws and fixtures were designed and fabricated to restrain and clamp the specimens during welding to maintain the root gap and minimize welding induced thermal distortions. The welding set-up is shown in Fig. 14. The double-sided arrows (yellow colored) in Fig. 14 represent the travel direction.

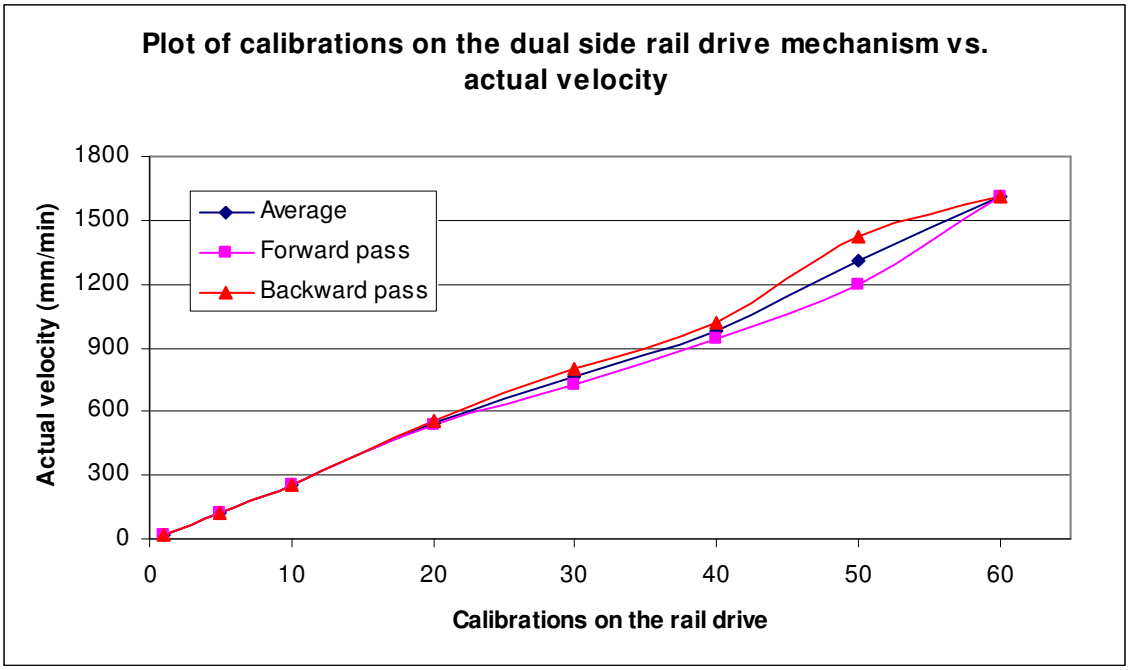

Fig. 13. Plot of actual velocity versus calibrations on the dual side rail drive mechanism.

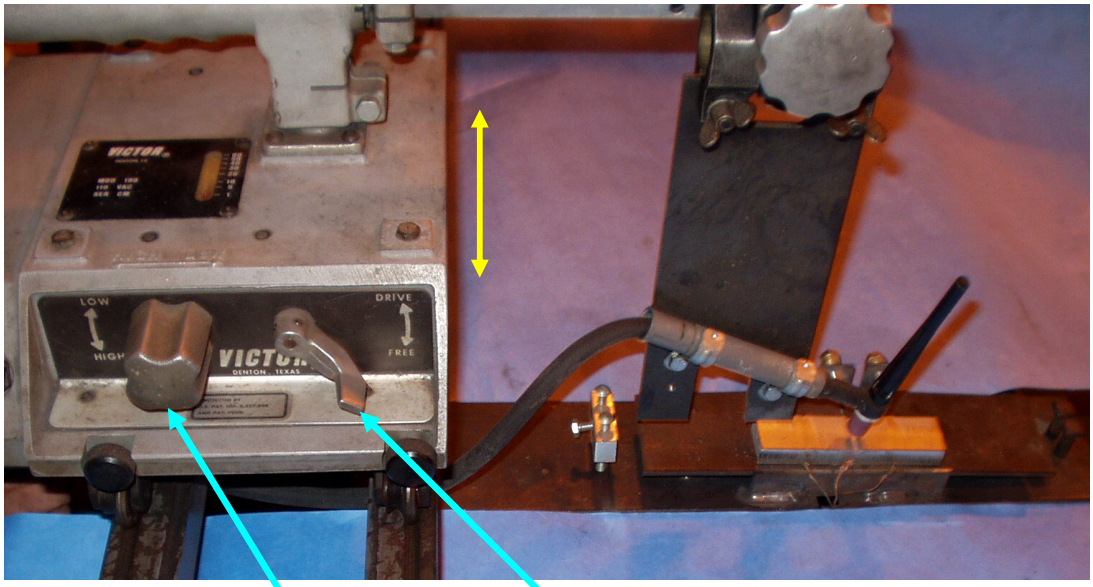

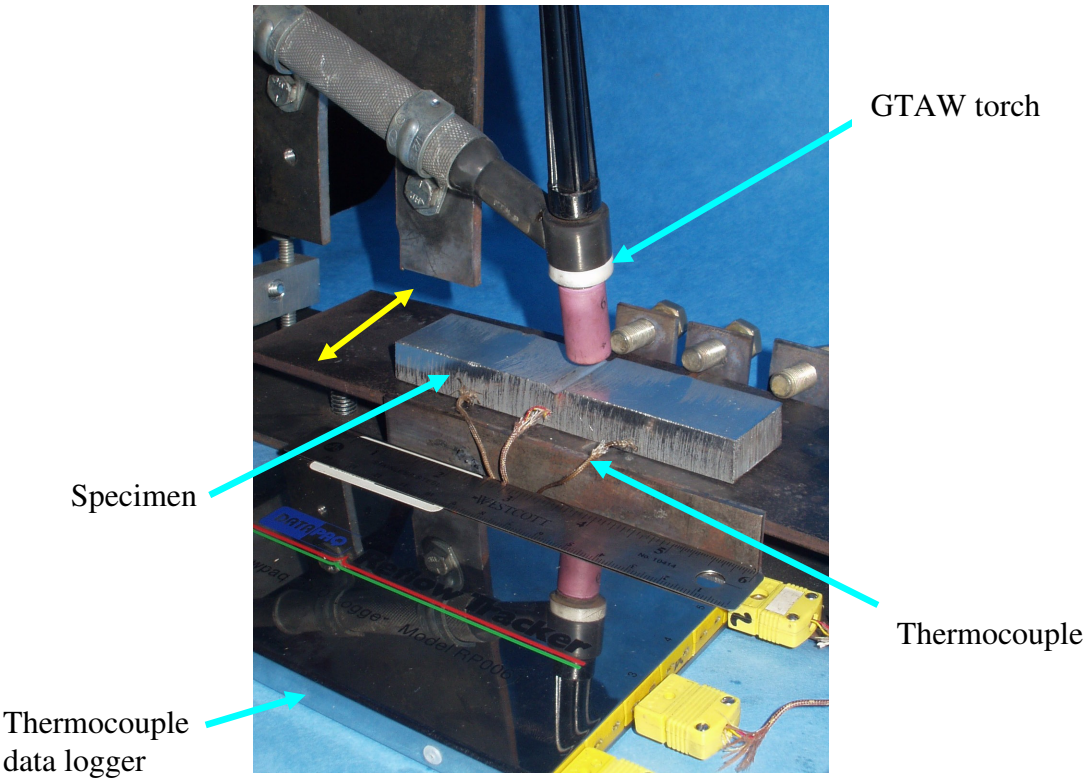

Fig. 14. Welding setup.

IV.5.2. Welding

1. Preliminary factorial tests

As per the test plan, after the specimens were milled according to the joint design shown in Fig. 10, they were cleaned with acetone to eliminate oil and grease and then mechanically cleaned with stainless steel brush to remove aluminum oxides. They were preheated on a hot plate to 150°C, measured with a K type thermocouple. Filler metal was added manually in the molten pool, and multiple passes were made to cover the entire region of the butt joint on each side.

2. Final factorial and optimized tests

The results as discussed later from the preliminary factorial tests necessitated few but major changes in the welding technique. It had become very important somehow to heat the material to a temperature high enough for welding for better fusion, but at the same time avoid the formation of oxides along the joint design.

The most important modification in these tests was that the specimens, after being preheated to 150°C, were also torch-heated at a distance (30 mm) from the weld joint on either side across the width of the specimen, as shown in Fig. 15. The torch was moved five times on location #1 while it was required to move it only twice on the other side at location #2 with the dual side rail drive mechanism. Multiple pass welds were made in the flat position for all the specimens, in which the first pass was with the addition of the filler rod, while the remaining passes were autogenous. The final and the optimized experiment were run at their respective welding conditions as mentioned earlier.

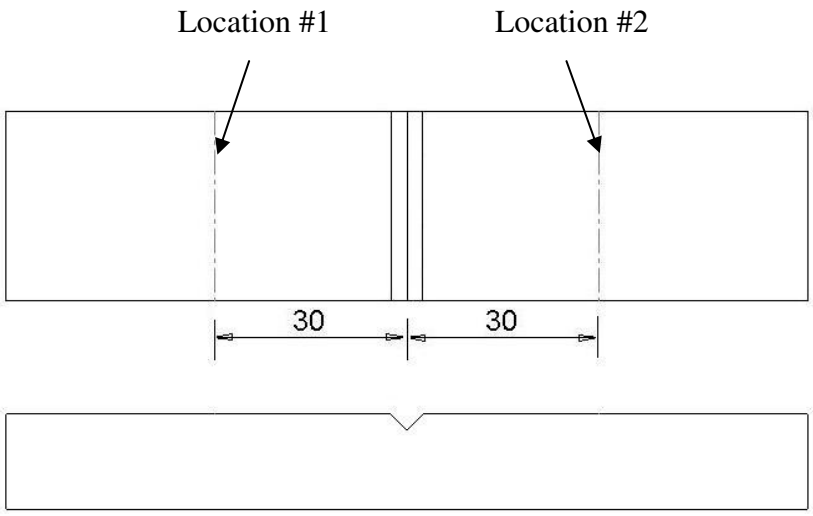

All dimensions are in mm

Fig. 15. Torch heating locations on the specimen before welding.

IV.5.3. Sample preparation for testing

1. Preliminary factorial test specimens

The specimens of the preliminary factorial tests were tested and analyzed for 1) Impact strength, 2) Microstructural condition, and 3) Microhardness. No replicates were made for any test run in the preliminary factorial tests since these were only screening tests. The welded specimens were milled to remove the excess weld metal. They were cut in two halves in a direction transverse to the welding direction with a sawing machine. One half was used for the Charpy V Impact test, while the other half was prepared for microstructural analysis and microhardness test. Fig. 16 shows a typical Charpy V test specimen as per AWS standards [12]; however only the V groove in the specimens was prepared according to the dimensions shown. The overall dimensions of the specimens were not as those shown in Fig. 16. For the microstructural analysis, metallographic sections were prepared from the tested specimens in a direction

perpendicular to the welding direction, and were ground and polished up to 1 µm finish. Abrasive papers of grit 240, 320, 400, and 600 were used sequentially for grinding. They were cleaned with water after the use of each grit paper and were blown dried using compressed air. They then were polished on a vibrating polisher, Buehler Vibromet 2, using diamond metallographic compound of 15 µm, 9 µm, 6 µm, and 1µm sequentially. They were cleaned with alcohol each time in the ultrasonic cleaner to remove the particles from the polishing surface. They were later etched with Keller's reagent {2 ml HF (48%), 3 ml HCl (conc.), 5 ml HNO_3 (conc.), and 190 ml of distilled water}. Keller's reagent is an etchant generally used to outline microconstituents and reveal grain boundaries for aluminum alloys [23]. The specimens were analyzed with optical microscopy on Olympus STM6 measuring microscope. They were later used for Vickers microhardness test on Buehler Micromet 2, Digital Microhardness Tester. The load used was 25 gm and was applied for ten seconds. The microhardness data points were taken across the weld zone, beginning from the weld center up to the unaffected base MMC.

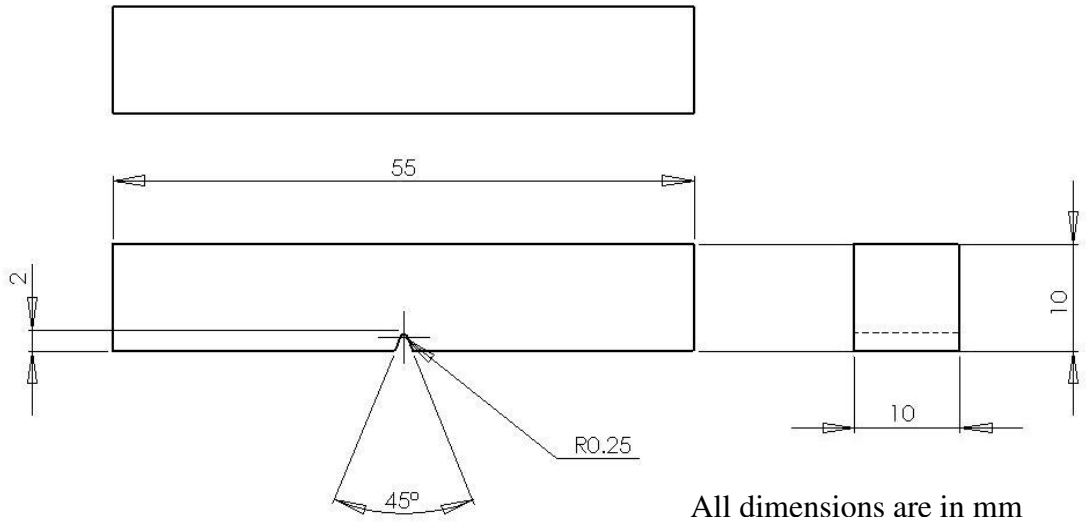

Fig. 16. Charpy V test specimen.

2. Final factorial test specimens

a. Tensile testing

The specimens were tested for their ultimate tensile strength by tensile testing on Universal testing machine, United Calibration Corporation, SFM 30. Three replicates for tensile testing were prepared to minimize errors. The specimens were not prepared like the standard dog-bone tensile specimen (Fig. 17), in order to avoid excessive machining close to the weld and avoid microcracks in the weld region. The notches in the tensile specimens (Fig. 18) were sawed in such a pattern that the tensile forces acting on it would be the same as those acting on a standard dog-bone shaped specimen. The tensile specimens prepared in this study represent one half of the standard dog-bone shaped specimen. To make these specimens comparable with the parent composites, the parent MMCs were also notched and tested in similar fashion. The weld specimens were tested transversely to the weld direction on a universal testing machine at a loading rate of 0.05 inch/min with the calibrated 2000 lbs. load cell. The load/displacement curves obtained were used to determine the extension corresponding to the ultimate tensile strength.

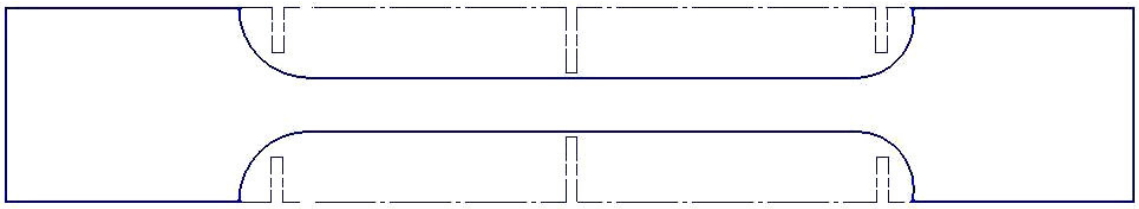

Fig. 17. Schematic representation for comparing standard dog-bone specimen with the actual prepared specimen for tensile testing.

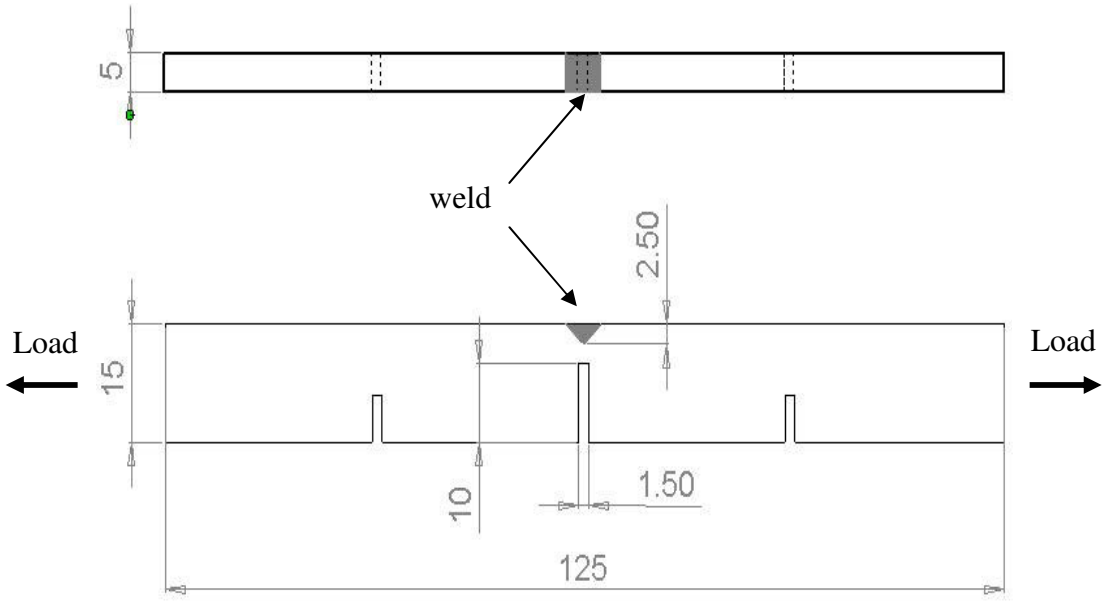

Fig. 18. Tensile test specimen.

b. Four point bending testing

All the specimens were tested by four point bending test (face bend test) on the same testing machine used for tensile tests. All the weld specimens were milled to blocks of size 125x30x15 mm, which was convenient for testing. The loading rate was again kept at 0.05 inch/min. Specimens for test run 3 and 4 of the final factorial test plan for (Table 6) were tested on a 30000 lb. load cell, while the specimens for test run 1 and 2 were tested with the 2000 lb. load cell, depending upon their dimensions. Fig. 19 shows the setup used for the test.

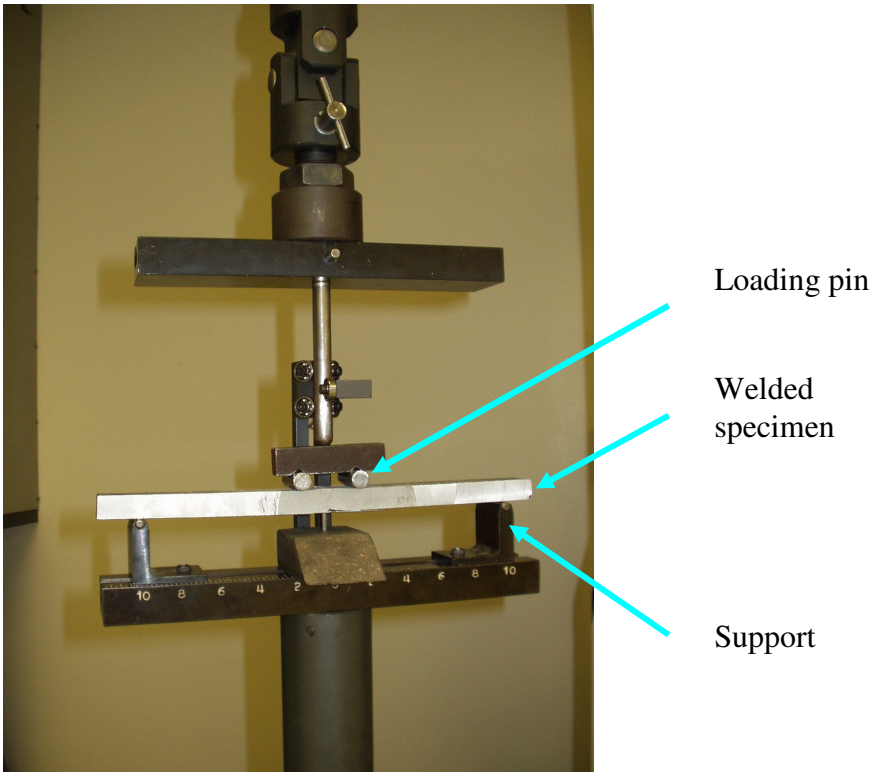

Fig. 19. Four point bending test setup.

3. Optimized test specimens

Three replicates were prepared for both, tensile and four point bending tests. After testing them, two out of the three replicates of each test were polished and etched in a manner similar to that of the preliminary factorial tests. They then were used for microstructural analysis using optical microscopy. Further, Vickers microhardness test was performed on one of the replicates of each destructive test.

IV.6. Finite element analysis

The finite element analysis (FEA) of this study was divided into two parts:

1. Predicting preheat temperature at the weld location
2. Predicting the weld pool temperature field

IV.6.1. Predicting preheat temperature

It was deemed necessary to find the temperature distribution across the MMC prior to the welding process due to preheating. It is known that the mechanical properties of the MMC degrade quickly at high temperatures. FEA was required to predict the preheat temperature to which the MMC should be heated to obtain a sound weld joint.

To compare and validate FEA results, temperatures were measured across the MMC experimentally during actual welding process. The temperature variation with time at three different locations was measured with K type thermocouples attached to the specimen during welding. Datapaq Reflowpaq 2000-model RP0061, temperature data logger, was used for acquiring the temperature from the thermocouples. Two thermocouples were located exactly below the two torch heating locations, 2 mm from the bottom surface, while the third thermocouple was located below the weld line, 5 mm from the bottom surface, as shown in Fig. 20. All the thermocouples were 3.5 mm deep in to the specimen, perpendicular to the page. The objective of this analysis was to find the temperature just below the weld line, i.e. 2.5 mm from the top surface, immediately before welding along the weld line. This location is marked as ‘A’ in Fig. 20.

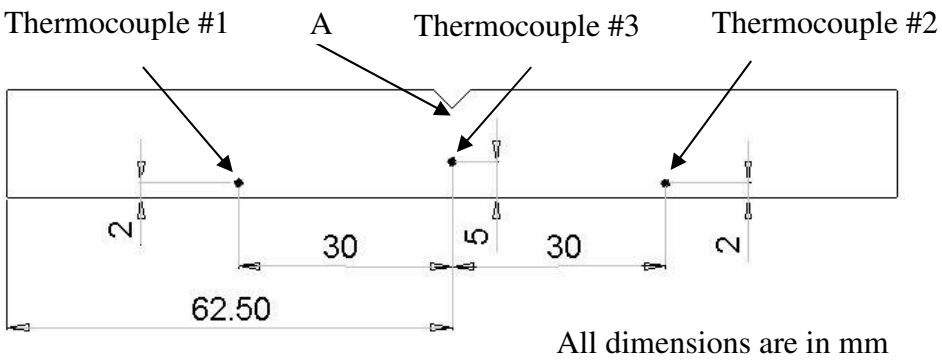

Fig. 20. Thermocouple setup during welding.

1. FEA model and mesh generation

A commercially available software ABAQUS, version 6.4 was used for FEA. The thermophysical properties used in the analysis were those of the MMC, as listed earlier in Table 9, which are the bulk properties of the MMC**.** Further, the volume fraction of SiC particles was only 10%. The model thus was constructed considering the MMC as a homogeneous isotropic metal. The model was drawn according to the dimensions of the actual specimen used. The heat loads at the two torch heating locations, #1 and #2 were applied on tapered strips on the specimen with dimensions as shown in Fig. 21. The strips were assumed to be tapered to take into account the effect of moving torch heat load.

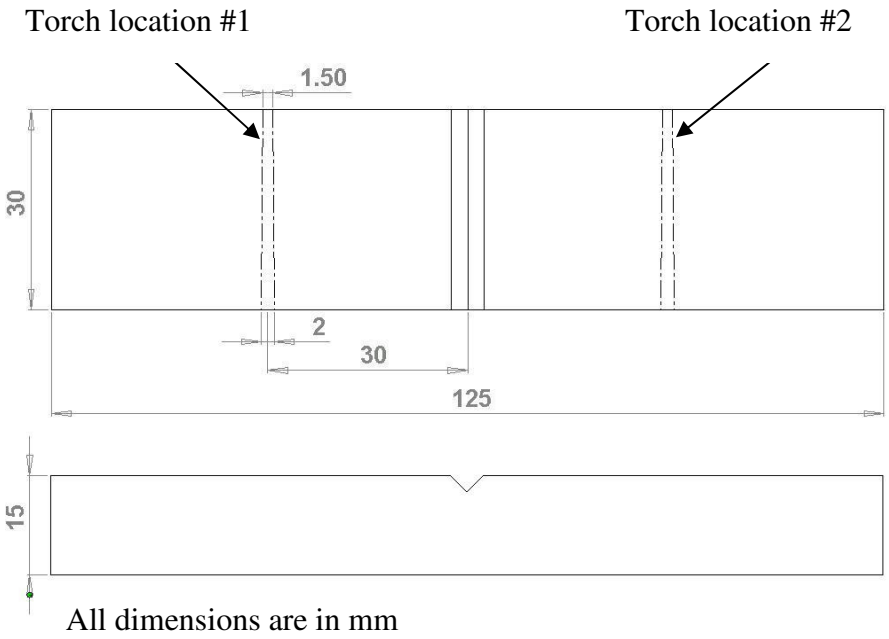

Fig. 21. FEA model for preheat temperature field.

A tetrahedral type of element was used to mesh the FEA model to suit the triangular geometry of the weld joint design. The mesh size was user-defined, wherein the mesh size was made finer along the joint design, the tapered strips and along the locations of the three thermocouples to get accurate results. The mesh generated is shown and discussed later, in the chapter "Results and Discussion'.

2. Assumptions

As mentioned earlier, the material of the FEA model was assumed to be homogenous and isotropic. Further, the heat transfer efficiency during welding was taken 70% [24], which means the fraction of the amount of heat generated at the torch tip transferred in to the specimen. The heat transfer coefficient used was 15 W/m^2 °K

[25] for all convective heat losses. Except the bottom surface, all the surfaces were subjected to convective heat losses throughout the analysis time. This is because the specimens were kept on a steel plate during actual experiments which also was preheated to 150°C and the heat losses from the bottom surface were neglected. Further, radiation losses were neglected.

3. Heat input and boundary conditions

The specimen was subjected to an initial boundary condition of 150°C. The heat loads were applied at the torch heating locations with an amperage of 90 A.

The heat energy obtained at the torch tip was calculated by:

$$\text{Power, } P = V \times I$$
$$= 14.5 \text{ Volt} \times 90 \text{ Amp.}$$
$$= 1305 \text{ W}$$

The heat input in the specimen was,

$$H = 0.70 \times 1305 \text{ W}$$
$$= 915 \text{ W}$$

This was the amount of heat input given at both the tapered strips during each torch heating. Since the torch was moved five times on the first torch heating location at 120 mm/min, the total time required was 95 seconds for traveling a length of 30 mm each time. Similarly, for the other side, it took 34 seconds to travel twice the width of the specimen. These time steps were obtained from the thermocouples attached to the specimen during actual welding and were fed in the FEA.

In between the above two heating steps, 14 seconds was the idle time, which was required to move and setup the torch from one location to the other. The ambient temperature was taken as 20°C (as measured by the thermocouple) throughout the analysis.

Thus, the following time steps were used in the entire FEA:

1. Heat input for 95 seconds on torch location #1
2. Idle time of 14 seconds
3. Heat input for 34 seconds on torch location #2

All these time steps were sequentially used in FEA and the temperatures profiles obtained at the thermocouple locations were then compared with the actual temperature measured.

IV.6.2. Predicting the weld pool temperature field

It was required to determine the temperature distribution in the weld pool to determine whether the interface reaction (1) occurs or not. The temperature field obtained then was compared with the critical temperature required for the interface reaction to occur, calculated on the basis of thermodynamic considerations.

The FEA model now used was without the V joint design, as shown in Fig. 22. This assumption was based on the fact that the composition of the filler rod was very similar to that of the MMC and the model was constructed as a complete block of MMC without a V joint design; however, the location of the V joint design was divided into three tapered strips for applying the heat loads, as shown in Fig. 22. Three strips were used, since in the actual experiments, three pass welds were made. Apart from these, other assumptions made were same as those of the above FEA simulation. Heat input and boundary conditions also were kept similar as in those used for predicting the preheat temperature. Time steps continued from the last time step of the above FEA simulation are described in the following paragraphs.

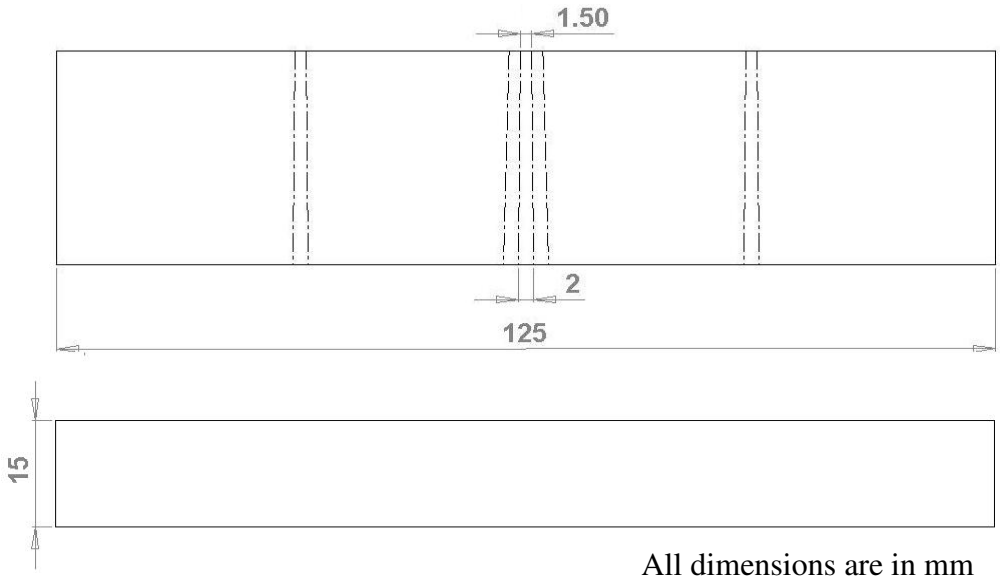

Fig. 22. FEA model for weld pool temperature field.

An idle time was given of 20 seconds, required to move and setup the torch from the preheating location to the actual weld joint location after the last time step of the previous simulation. Following that was applied a heat load along the three tapered strips at the location of the V joint design. The heat load of magnitude 915 W, as calculated above, was applied once along each tapered strip. The total time for this time step was 31 seconds for traveling a length of 30 mm each time at a speed of 260 mm/min (optimized level of the welding speed). Further, an arbitrary idle time step of 300 seconds was applied to simply see how the temperature drops across the weld pool region after the removal of the heat load.

To summarize, following were the total time steps applied in this simulation:

1. Heat input for 95 seconds on torch location #1
2. Idle time of 14 seconds
3. Heat input for 34 seconds on torch location #2
4. Idle time of 20 seconds
5. Heat input for 31 seconds on the weld joint
6. Idle time of 300 seconds

The temperature field obtained across the weld pool from this simulation was used to find out the probability of the occurrence of the Al-SiC interface reaction in the weld pool region.

CHAPTER V

RESULTS AND DISCUSSION

V.1 Preliminary factorial experiments

V.1.1. Charpy Impact test

The Charpy Impact test results are tabulated in Table 12. It was seen that the impact strengths varied only to a small extent; however, it was seen that high heat inputs as in specimen for test run #8 resulted in low impact strengths and low heat inputs in specimens as for test run #7 had higher impact strengths. Further, specimens with wider weld joint designs such as for test run #7 had slightly higher impact strengths as those with narrower weld joint designs such as for test run #3, with levels of other factors remaining the same. This probably could be due to slightly better penetrations (though not complete penetration) in specimens with wider joint designs. Since only one replicate was tested at each test run, these variations might not reflect the true influence of the welding variables. More replicates might help understanding the results better.

The fracture propagation in all the specimens was found to be along the joint design and not along the weld metal region. This was due to lack of fusion of the filler metal with the base MMC along the joint design. When the fractured surfaces were carefully observed, it also was found that all the specimens had incomplete penetration. Even though the specimen were welded by a double-V butt joint, the penetration was not sufficient to weld the entire thickness of the specimen. Further, there were layers of oxide between the filler metal deposited and the base MMC along the joint design. It is important to note that these values did not depict the actual impact strengths of the weld specimens, but were used relatively to understand the influence of the welding variables.

Table 12

Charpy Impact test results for preliminary factorial test runs

Test Run	Welding current	Welding speed	Weld joint design	Impact Strength (Joules)
1	-	-	+	8.5
2	+	+	+	7.6
3	-	+	-	7.5
4	+	+	-	6.9
5	+	-	+	7.4
6	-	-	-	7.7
7	-	+	+	8.9
8	+	-	-	6.4

V.1.2. Microstructural analysis

The specimens when analyzed with optical microscopy gave a better understanding of the impact test results. Fig. 23 shows a microstructure of the specimen welded with a 75° V joint angle, and at 90 A and 250 mm/min. The microstructure showed distinct regions, viz. region I, region II, the HAZ, and finally the unaffected base MMC. Region I was filler metal rich, seen right at the center of the weld, due to the addition of the filler metal, and comprising the maximum part of the weld region. The concentration of SiC particles in this region in almost all the specimens was negligible. Surrounding it was seen region II, which had high concentrations of SiC particles and oxides. This region was formed due to the exposure of the base MMC to the atmosphere at high temperatures. The filler metal rich zone was enclosed in a skin of oxides and SiC particles. Such non-uniform distribution of SiC particles across the weld zone and the

dilution of the composite in region I caused all the specimens to fracture along the joint design in the impact test. This not only led to lack of proper fusion, but also increased the porosity levels in the weld metal region. Further, it is evident that the weld did not completely penetrate through the thickness of the specimen. The HAZ surrounded region II. The extent of this region was hard to find in the microstructure, since it might be very narrow due to low thermal cycles and low temperature ranges across the weld.

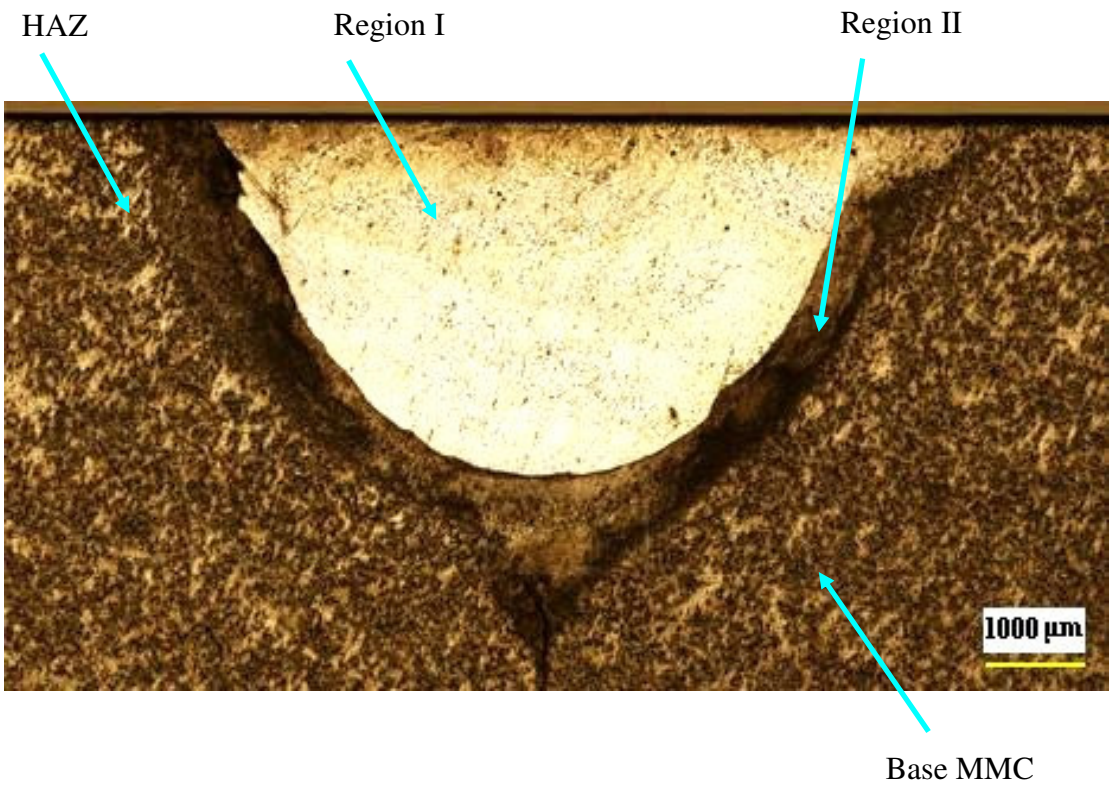

Fig. 23. Microstructure of a specimen welded with 75° V joint angle, at 90 A and 250 mm/min, showing distinct zones.

All the specimens of the preliminary tests had similar regions in their weld microstructure. The only change was in the width of the HAZ. Though they were not studied in depth, it could be seen that higher heat inputs led to wider HAZ.

V.1.3. Vickers microhardness test

The specimen when tested for Vickers microhardness test had variations in the microhardness values due to the presence of different zones as explained above. Fig. 24 shows the variation of microhardness values across the weld for test run #2 (Table 5). Region I, the filler metal rich zone, had a range of hardness values, with an average of 80 Vickers hardness number (VHN). Region II had high hardness values, in the range of 110-160 VHN with an average of 130 VHN, probably due to the hard SiC particles and the brittle eutectic phase of Al-Si, rather than the soft metal matrix. The HAZ had hardness values similar to those of the base MMC, with an average of 70 VHN. The small drop in the hardness values might be due to a measurement error during hardness testing. One also might think that, as as-cast components when welded do not have extensive grain growth, their hardness values do not drop considerably.

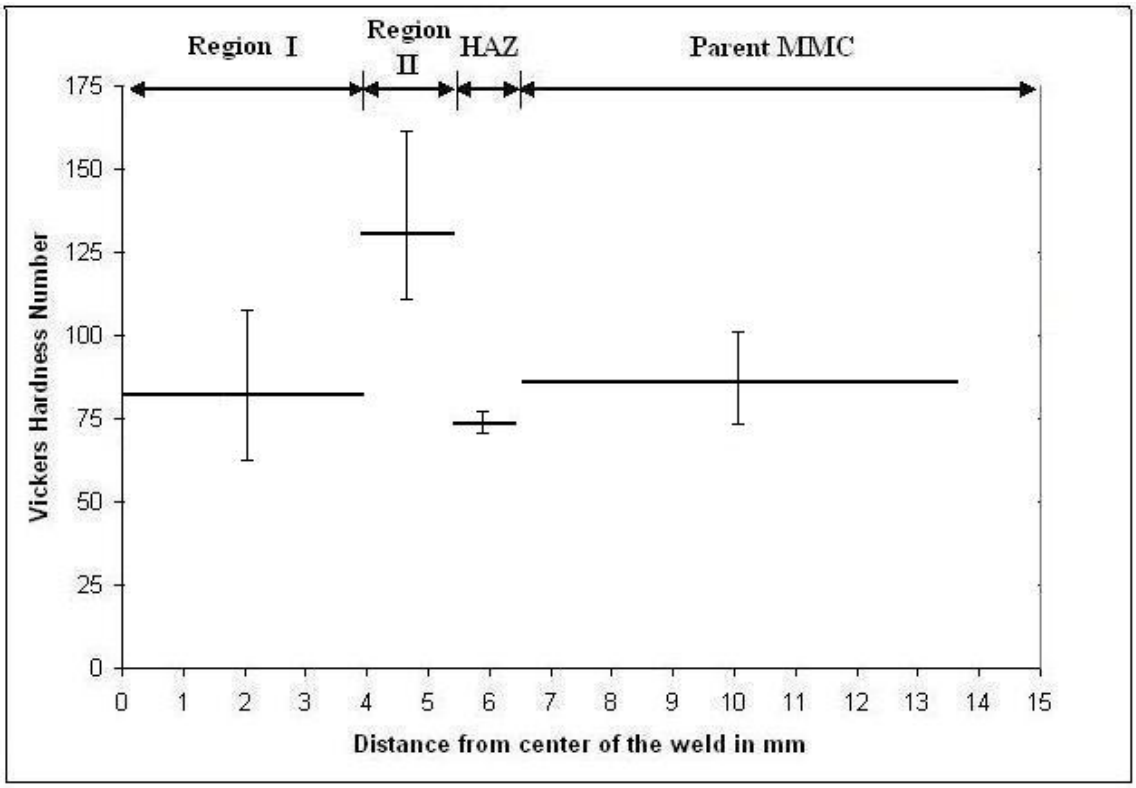

Fig. 24. Variation of VHN across the weld, tested by 25 gm and for 10 seconds, of a specimen with 75° V joint angle run at 110 A and 250 mm/min.

From the above results, it was concluded that the welding technique and the weld design needed to be modified to avoid the formation of two different zones within the weld zone. Also, it was required to remove the oxides or even completely prevent their formation during welding. Complete fusion between the filler metal and the base metal was paramount to achieve sound welds and maintain weld integrity.

V.2 Final factorial experiments

V.2.1. Tensile testing

The notched parent MMCs were tested for their ultimate tensile strength and their values were calculated. It is important to note that the tensile strengths obtained from the tests were not the actual strengths of the material, as they were notched underneath the weld, as explained earlier; however, since all the specimens were tested in the same manner, it gave a relative understanding of their variations. They later were multiplied with a stress concentration factor to get the actual induced tensile stresses.

The tensile strengths obtained from the tensile testing of the notched welded specimens of the final factorial tests varied significantly, depending upon the test run conditions. This implied that both welding current and welding speed were significant welding process variables. Also, since three replicates were tested at each test run, a range of tensile strength values for each test run was obtained. The position of the failure crack varied from either the weld metal zone or along the joint design. As expected, those weld joints failing in the weld metal zone had a higher range of tensile strengths, while those failing along the joint design had lower strength values. Further, it also was seen that the parent MMCs had little % elongation of 4-4.75%, being brittle in nature.

The tensile stresses were calculated using equation (3):

$$\sigma = \frac{P}{A} \tag{3}$$

where P is the breaking load and A is the area of cross section in loading.

For instance, for specimen #1b, it would be as follows: $P = 2112$ N; $A = 31.2$ mm^2

$$\therefore \sigma = 67.69 \text{ MPa}$$

Since the specimens were notched below the weld, all the values obtained by equation (3) were multiplied by a stress concentration factor [26], which was calculated as follows:

$$\text{Stress concentration factor, } K_t = C_1 + C_2(\frac{h}{D}) + C_3(\frac{h}{D})^2 + C_4(\frac{h}{D})^3 \qquad (4)$$

where

$$C_1 = 0.953 + 2.136\sqrt{\frac{h}{r}} - 0.005(\frac{h}{r})$$

$$C_2 = -3.255 - 6.281\sqrt{\frac{h}{r}} + 0.068(\frac{h}{r})$$

$$C_3 = 8.203 + 6.893\sqrt{\frac{h}{r}} + 0.064(\frac{h}{r})$$

$$C_4 = -4.851 - 2.793\sqrt{\frac{h}{r}} - 0.128(\frac{h}{r})$$

and h, r, and D are as shown in Fig. 25.

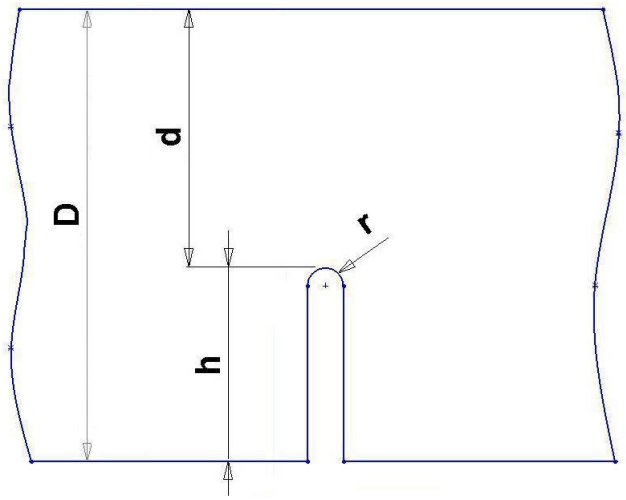

Fig. 25. Geometry for calculating stress concentration factor.

Substituting h = 10 mm, r = 0.75 mm, and D = 15 mm as from Fig. 18 in the above equations, the stress concentration factor, $K_t = 2.07$

Therefore, the actual ultimate tensile stress in specimen #1b,

$$\sigma_{UTS} = 2.07\sigma \qquad (5)$$
$$\approx 140 \text{ MPa}$$

The % elongation was calculated as:

$$\% \text{ elongation} = \frac{\Delta L}{L} \times 100 \qquad (6)$$

where L is the original gauge length and ΔL is change in the gauge length after testing
For specimen # 1b, L = 60 mm; $\Delta L = 1.579$ mm

$$\therefore \% \text{ elongation} = \frac{1.579}{60} \times 100$$
$$= 2.63$$

Similarly, all the stresses were corrected by the stress concentration factor and the % elongation were calculated, as summarized in Table 13.

Table 13

Final factorial experiments - tensile test results (three replicates each)

Run		**Welding current**	**Welding speed**	σ_{UTS} **(MPa)**	**% of parent** σ_{UTS}	**% elongation**	**% of parent elongation**
1	a	+	-	138	57	2.6	60
	b			140	58	3.71	85
	c			191	79	4.7	107
2	a	+	+	155	64	3.5	80
	b			166	69	4.6	105
	c			218	90	5.2	119
3	a	-	-	174	72	4.35	100
	b			203	84	4.98	114
	c			218	90	5.4	123
4	a	-	+	196	81	4.45	102
	b			205	85	4.98	114
	c			223	92	5.5	126
Parent MMC				242	100	4.38	100

V.2.2. Four point bending testing

The parent as-cast MMC was tested in four point bending test and its bending strengths along with its bending strain were calculated. Once again, the bending strains were very low due to the brittle nature of the parent MMC. Similarly, the bending strengths of the welded specimens of the factorial tests and their corresponding strains were calculated. The bending stresses for all the specimens were calculated based on the loading diagram as shown in Fig. 26.

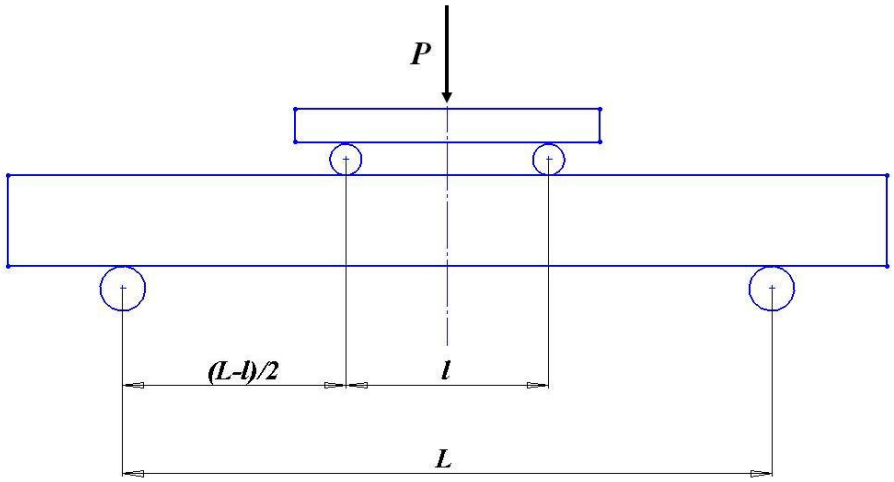

Fig. 26. Bending load diagram.

The bending stress was calculated as shown:

Bending stress,

$$\sigma_b = \frac{P \times (L - l) \times y}{4I} \tag{7}$$

where P = Breaking load

L = Bending span length

l = Uniformly distributed load length

I = Area moment of inertia

y = Distance from the neutral axis up to the outermost layer of the specimen in tension

For instance, for the parent specimen,

P = 6205 N; Area of cross section, A = 28.58 x 10.81 mm^2; L = 127 mm (5 inch);

l = 38.1 mm (1.5 inch); $y = \frac{10.81}{2} = 5.41$ mm

$$\therefore \sigma_b = \frac{6205\times(127-38.1)\times12\times5.41}{4\times28.58\times10.81^3}$$

$$\approx \text{ 248 MPa}$$

Similarly, the bending strain was calculated using the geometry of the specimen in bending as shown in Fig. 27.

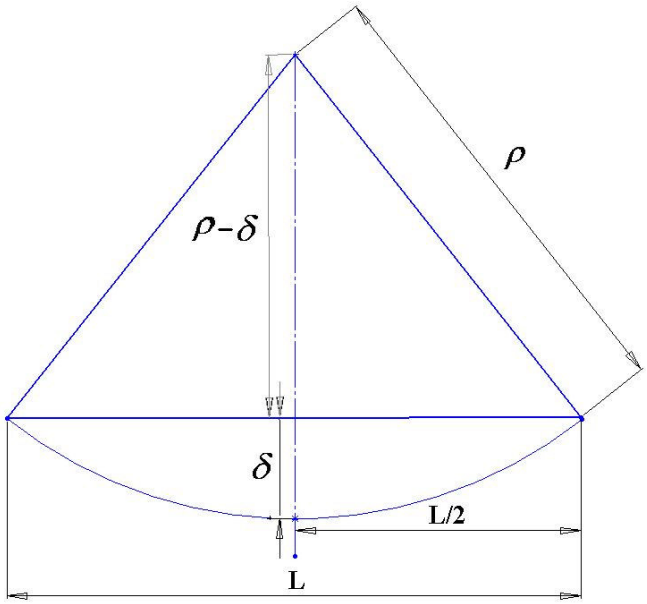

Fig. 27. Specimen geometry in bending.

The radius of curvature ρ was calculated from the following:

$$\rho^2 = (\rho-\delta)^2 + \frac{L^2}{4} \tag{8}$$

$$\therefore \rho = \frac{L^2}{8\delta} \tag{9}$$

where δ is the deflection corresponding to failure.

For the parent specimen,

δ = 4.0716 mm (0.1603 inch)

$$\therefore \rho = \frac{127^2}{8 \times 4.0716}$$

$$= 495.16 \text{ mm}$$

Thus, bending strain ε is given by,

$$\therefore \varepsilon = \frac{\delta}{\rho} \qquad (10)$$

$$= \frac{4.0716}{495.16}$$

$$= 0.822\%$$

Similarly, all the stresses and strains were calculated and are tabulated in Table 14. It is seen that the bending strain for the specimens for test runs #2 and #3 are very close to those of the parent MMCs. This is because these specimens failed in their base metal region**,** resembling brittle fracture mode, while the remaining two specimens for test runs #1 and #4 failed in the weld region, giving higher bending strains. Specimen for test runs #3 and #4 were tested with a 30000 lbs. load cell, which was not calibrated, and their bending strength values should not be taken in the absolute sense. The load cell was not possibly able to accurately measure low range of loads and predicted high strengths.

Table 14

Final factorial experiments - four point bending test results (single replicate each)

Run	Welding current	Welding speed	Bending strength (MPa)	% of parent strength	% Bending Strain	% of parent bending strain
1	+	-	199	80	2.39	290
2	+	+	210	85	1.06	129
3 *	-	-	296	100	1.36	165
4 *	-	+	294	100	2.84	345
Parent MMC			248	100	0.822	100

* Note: Data collected with an un-calibrated 30000 lbs. load cell.

V.3 Design of experiments – results and analysis

Design Expert, DX6, version 6.0, a commercial software for analyzing designed experiment and their results, was used to understand the influence of the welding variables on the weld properties. Since the bending test results were not accurate, they were not fed in the software and only tensile test results were used for further analysis. A two level factorial test design was selected in DX6. It was a three replicate design since results of three replicates of tensile tests were to be fed. The tensile strength was the response variable and the optimization condition was to achieve maximum tensile strengths.

The results from the analysis implied that both the factors were significant variables. Fig. 28 shows the variation of tensile strength with current and speed. It is seen that tensile strengths increases with decreasing values of welding current and increasing values of the welding speed.

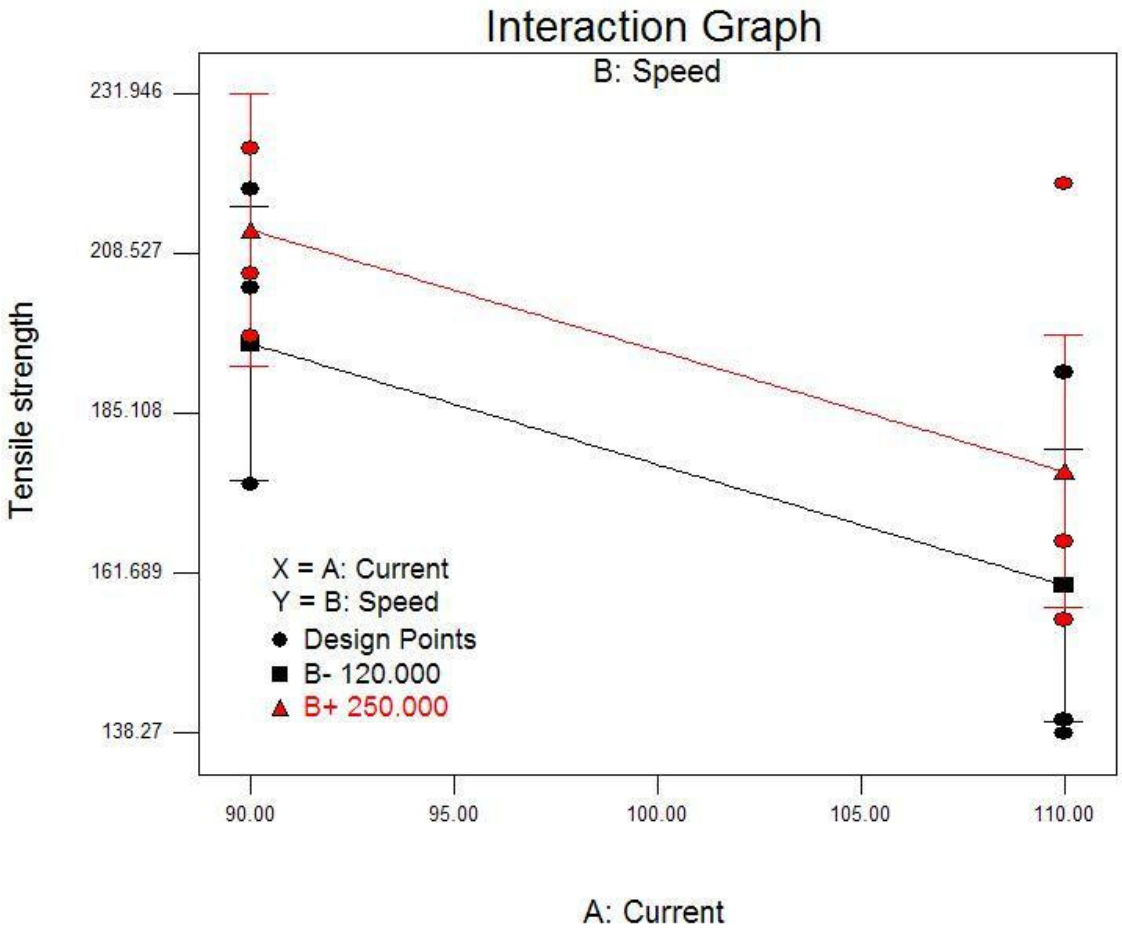

Fig. 28. Interaction graph; tensile testing.

As mentioned in the earlier chapter, the optimized condition obtained from the software analysis was to set the welding current at 85 A and the welding speed at 260

mm/min. This was expected as it was seen from the results of the tensile tests and the interaction graphs that weld strengths had an upward trend at lower currents and higher speeds.

V.4 Optimized experiment

V.4.1. Tensile and four point bending tests results

The tensile and four point bending test results of the experiments run at the optimized conditions are listed in Tables 15 and 16, respectively. The results obtained with these tests were found to match closely with the predicted values by Design Expert. The ultimate tensile strength was found to be approximately 85% of the parent material properties. Similar in the bending tests, the strength was found almost equaling the parent strength. Further, the failure was located in the weld metal or in the HAZ (one of the bending specimen) and not along the joint design. This implied that the optimized welding conditions were appropriate for a sound weld joint and that the amount of penetration transverse to the joint design was high enough to fail the specimen either in the weld metal region or in the HAZ. The results were better understood when they were analyzed with optical microscopy which are explained later.

The % elongation of the tensile tested specimens was found to be higher than those of the parent MMC. Similarly, the bending strains were found to be more than the corresponding parent MMC strains. This can be explained on the fact that the as-cast MMCs are brittle in nature; however, with the addition of Al-Si filler metal during the welding process, the ductility of the specimen increases, leading to higher elongations.

Table 15

Optimized experiment - tensile test results (three replicates each)

Run	σ_{UTS} **(MPa)**	**% of parent** σ_{UTS}	**% elongation**	**% of parent elongation**
a	199	82	6.0	137
b	202	83	5.2	118
c	217	90	7.0	160
Parent MMC	242	100	4.38	100

Table 16

Optimized experiment - four point bending test results (three replicates each)

Run	σ_{UTS} **(MPa)**	**% of parent** σ_{UTS}	**% Bending strain**	**% of parent bending strain**
a	244	100	1.1	133
b	268	108	1.27	155
c	278	112	1.5	182
Parent MMC	248	100	0.822	100

V.4.2. Microstructural study

Optical microscopy revealed that the welding process altered the weld microstructure. Two zones were identified, the weld metal zone and the HAZ, before reaching the unaffected base metal. The weld metal zone could be distinguished in three regions; viz. Region A, B, and C as shown schematically in Fig. 29. Region A once again was filler rich zone, at the top center of the weld. Region B had uniform mixture of

the filler metal and the base metal with SiC particles distributed in it. Region C, which was well below the joint design, was rich in base metal. Surrounding this region was the HAZ. One quick observation to be made is that the region II, which was the oxide and SiC-rich zone obtained in the earlier preliminary factorial tests (Fig. 23) now was replaced by region B and C. Further, the filler metal rich zone which covered the majority of the weld region earlier now was reduced to a very small region at the top of the weld.

1. Tensile specimens

Figs. 30 and 31 illustrate the microstructures of two different replicates of the tensile tested specimens. Each figure shows one half of two different specimens. In both the specimens, the failure was seen in the weld region. The microstructures of the different zones are explained later.

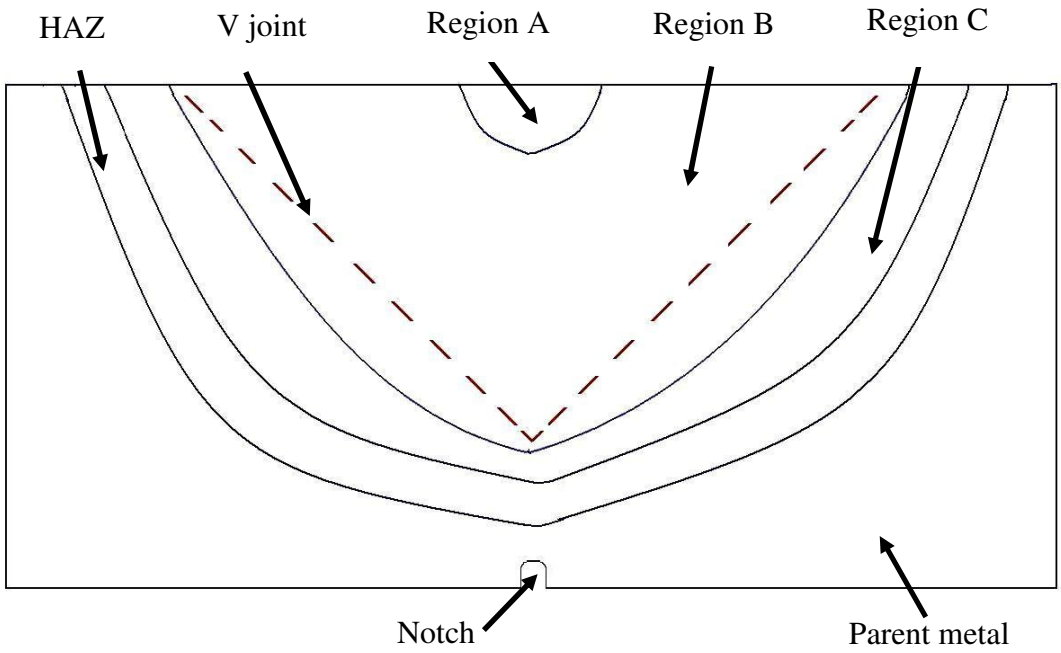

Fig. 29. Schematic representation of the weld.

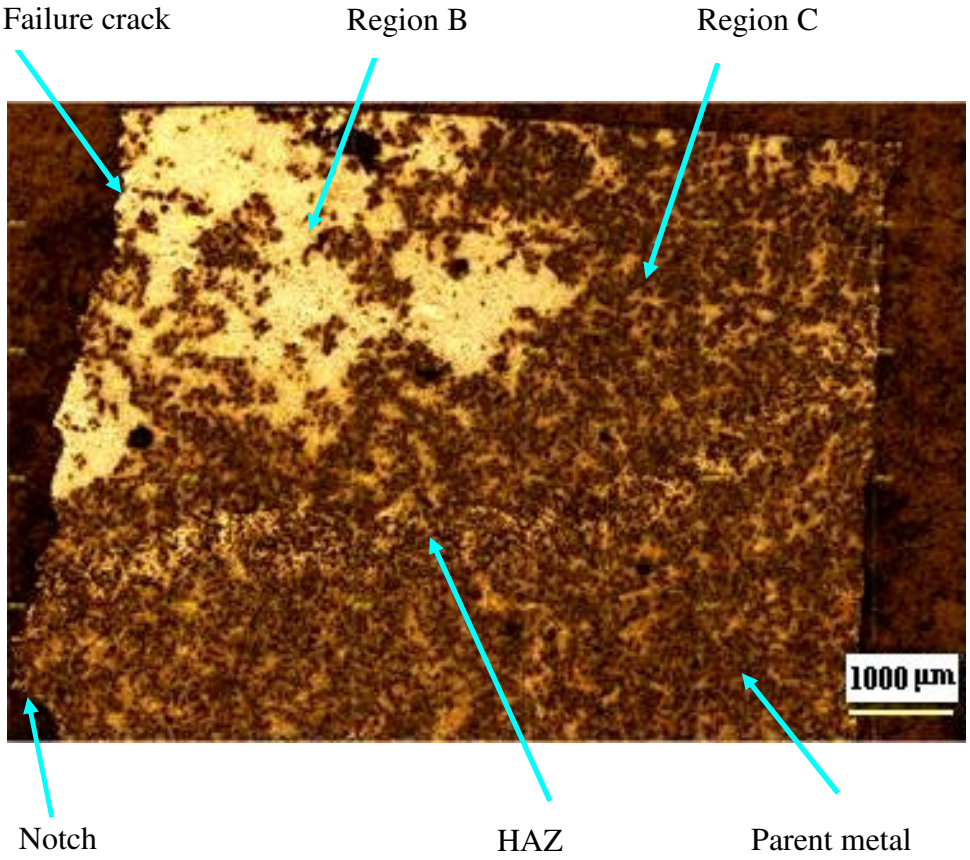

Fig. 30. Microstructure of the right half of tensile tested specimen #1 (Fig. 29), welded at optimized conditions (85 A and 260 mm/min).

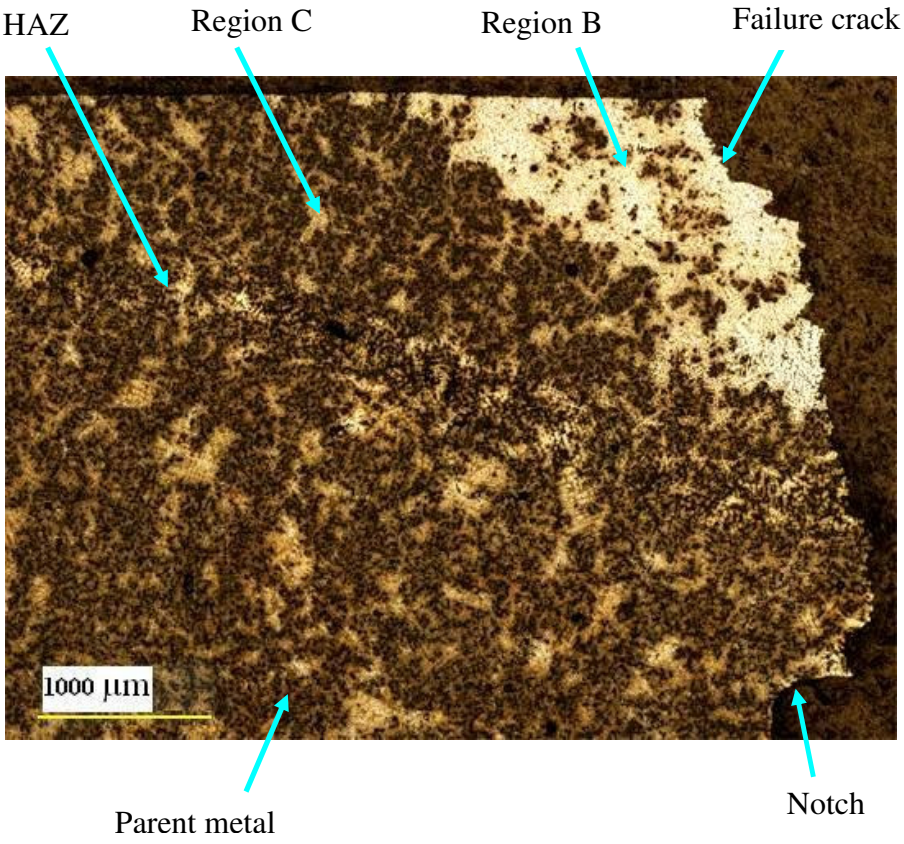

Fig. 31. Microstructure of the right half of tensile tested specimen #2 (Fig. 29), welded at optimized conditions (85 A and 260 mm/min).

2. Bending specimens

Similarly, Figs. 32 and 33 illustrate the microstructures of specimens tested in four point bending test. Fig. 32 shows that the specimen failed in the region along the HAZ and the unaffected base metal. The specimen shown in Fig. 33 failed in the weld region.

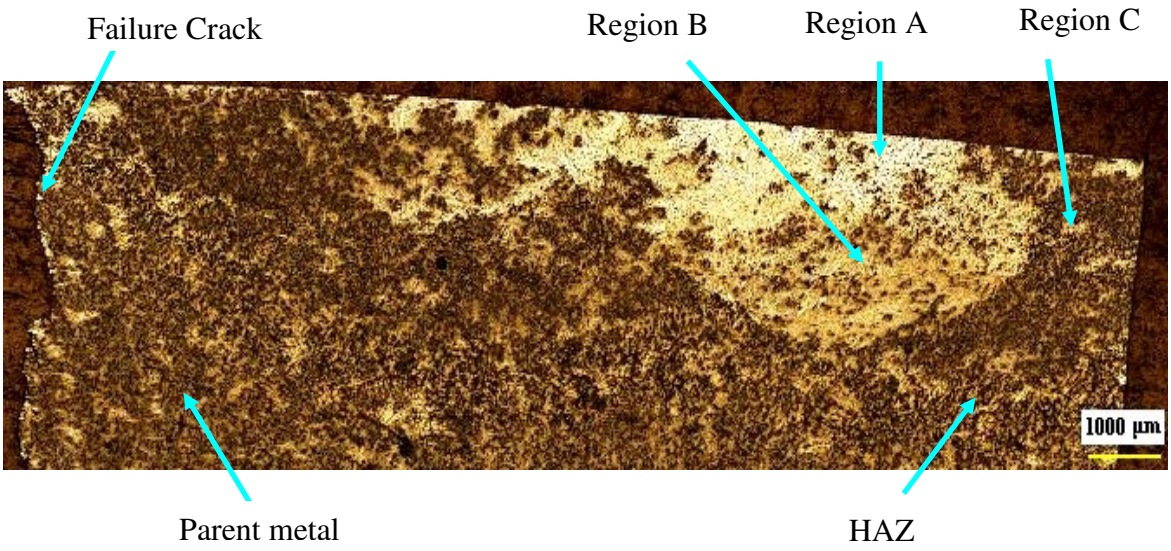

Fig. 32. Microstructure of one half of specimen #1 tested in bending, welded at optimized conditions (85 A and 260 mm/min).

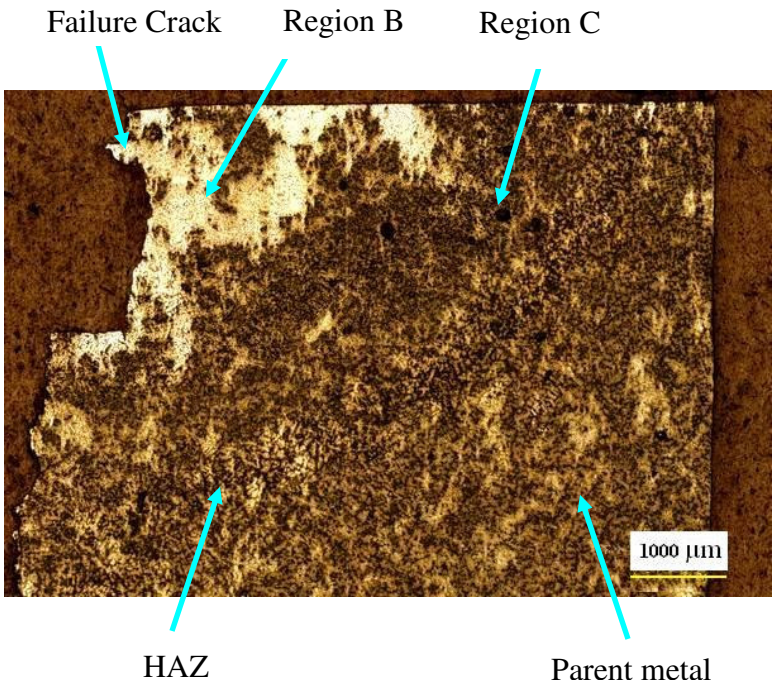

Fig. 33. Microstructure of right half of specimen #2 tested in bending, welded at optimized conditions (85 A and 260 mm/min).

The microstructures of all the above specimens shown in Figs. 30, 31, 32, and 33 revealed the zones as described in Fig. 29. Region A, which is the filler metal rich zone, is not seen in Figs. 30, 31, and 33 since the weld failure in all these specimens was along region A. The microstructure in this region and to some extent in region B was finest due to higher cooling rates along the weld line. Due to low currents and controlled heat inputs, the interface reaction between SiC particles and molten aluminum did not occur and no instances of aluminum carbide flakes were found.

As mentioned earlier, region C had a higher dilution ratio, which is defined as the ratio of the amount of the volume of base metal i.e. the MMC to that of the weld metal (Region A, B, and C combined), due to more contribution from the base MMC. This is due to the viscous effects of the molten pool, because of which there was comparatively less stirring action in this region and consequently did not mix with region B. This also is based on the fact that some of the particles which are at the extreme bottom of the molten weld pool of region B may have sunk further below during solidification, lying in region C. Thus, its microstructure resembled closely to that of the base material. Once again, the formation of aluminum carbide needles was suppressed in this zone. It was difficult to calculate the dilution ratio in the above welds since the composition changed significantly from one region to other.

Fig. 34 shows the weld zone microstructure (region B) of a tensile specimen at a higher magnification. It once again was seen that the SiC particles always solidify in the eutectic region of Al-Si, which solidify in the end during welding, similar to that of the casting process. The reinforcements were pushed ahead of the solidification front, segregating in the eutectic region. Further, it also was inferred that the failure crack propagated along the eutectic phase, since it was more silicon rich and less ductile than the aluminum-silicon matrix, as shown in Fig. 35.

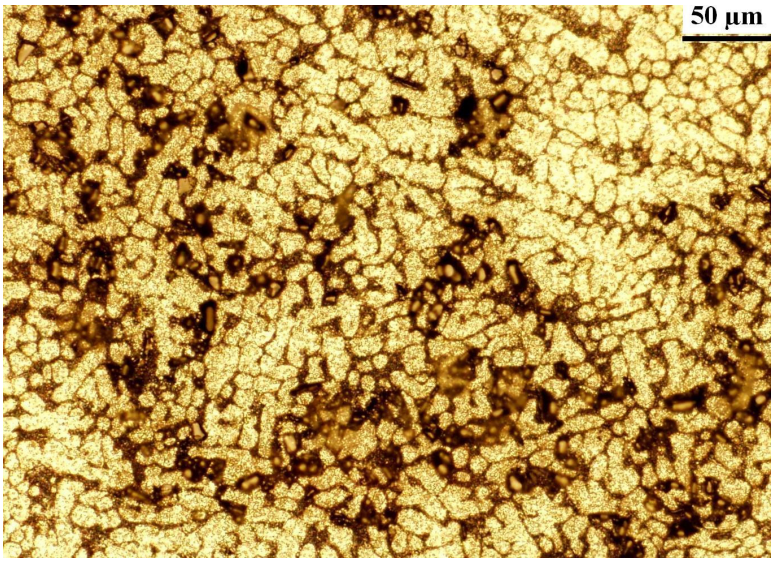

Fig. 34. Microstructure of region B of tensile specimen #1 welded at optimized conditions (85 A and 260 mm/min), at a higher magnification.

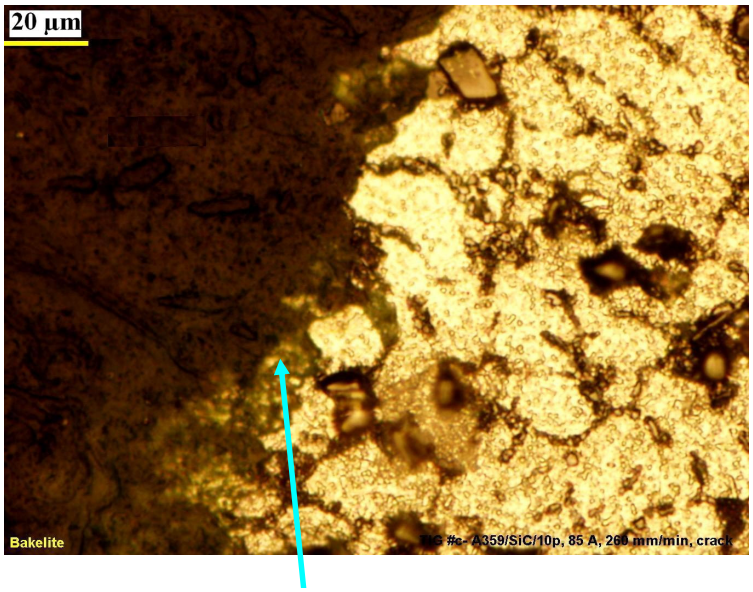

Brittle Al - Si eutectic phase

Fig. 35. Failure propagation along the brittle Al-Si eutectic region in a specimen welded at optimized conditions (85 A and 260 mm/min).

Instances of voids and porosities were found, both in the base metal and the weld metal region. Voids were more prone in the base metal region, which are common in cast components due to solidification defects. Porosities, inherent in arc welding, were prominent in region C, as shown in Fig. 36. Interdendritic porosity was formed during the solidification process. This mainly was due to the low wettability of the SiC particles with aluminum matrix during welding. As known, porosities reduce the weld strengths and the ductility depending on their amount.

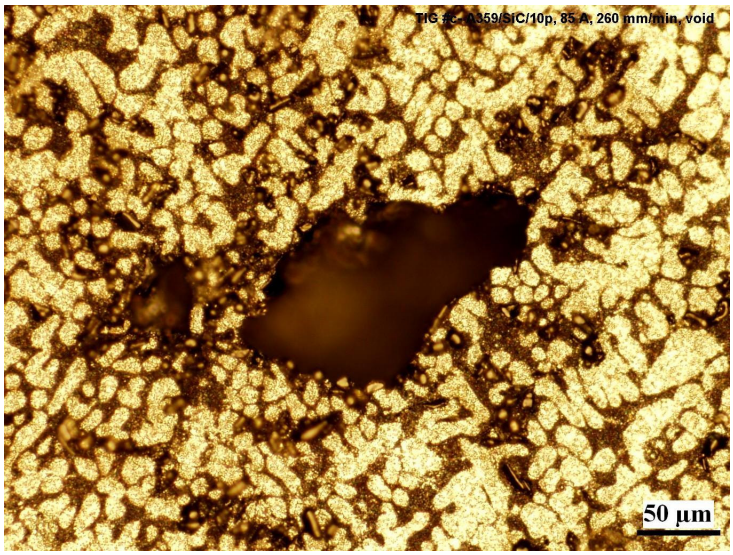

Fig. 36. Interdendritic porosity in region C of a specimen welded at optimized conditions (85 A and 260 mm/min).

The high tensile and bending strengths obtained at low level of welding current and high level of welding speed now can be explained. With low currents and high welding speeds, the weld pool is in a molten state for a comparatively lesser amount of time. Due to this, the SiC particles have less time to redistribute themselves and their

probability to sink to the bottom of the weld pool reduces. The pool quickly solidifies and majority of the SiC particles remain in region B itself. This uniform distribution of the SiC particles in the weld metal zone contributes strength to the weld joint.

Weld strengths also are related to the level of interface reaction (1), which is directly proportional to the amount of heat input. Excessive currents will overheat the pool and lead to the formation of aluminum carbide, which are brittle in nature. With their formation, the volume fraction of SiC particles reduces, leading to the degradation of the composite properties. Also, their formation is dependent upon the welding speed and the cooling rates. In the optimized conditions, due to high welding speeds, their formation was suppressed since the total welding heat input is inversely proportional to the welding speed. Addition of Si from the filler metal further helps in avoiding the formation of Al_4C_3 flakes. According to reaction (1), the addition of Si will increase the content of Si in the welding pool, reversing the reaction direction and suppressing the formation of Al_4C_3 flakes.

Explanation on the conditions favorable for the interface reaction can also be given, based on thermodynamic considerations as follows:

The free energy change (J/mol) for reaction (1) is given by [1]:

$$\Delta G = 113900 - 12.06\, T \ln T + 8.92 \times 10^{-3}\, T^2 + 7.53 \times 10^{-4}\, T^{-1} + 21.5\, T + 3\, RT \ln a_{[Si]} \qquad (11)$$

where $a_{[Si]}$ is the activity of Si in liquid Al
R is the gas constant in J/mol °K
T is the absolute temperature (°K)

The activity of Si in liquid Al, $a_{[Si]}$ is known to be approximately 0.1 for A356/SiC MMCs [17]. As mentioned earlier, the filler metal used in this study was R-A356.0, which has a chemical composition similar to the matrix composition of the A356/SiC

MMC. The matrix composition of the parent metal in consideration, A359/SiC/10p, was slightly different from the above alloys; however, the probability of the interface reaction (1) was higher in region B (due to presence of SiC particles) of the weld metal which, as explained earlier, had equal contributions from both filler metal and base metal, leading to a composition in between that of A356 and A359 alloy. It thus was a reasonable approximation to use the above value as 0.1 in this study. Substituting this value in equation (11) and R as 8.314 J/mol °K**,** we get:

$$\Delta G = 113900 - 12.06\, T \ln T + 8.92 \times 10^{-3}\, T^{2} + 7.53 \times 10^{-4}\, T^{-1} - 35.93\, T \qquad (12)$$

To find whether reaction (1) occurs or not, the above equation was iterated for different values of temperature, *T*, to find the variation of ΔG with *T*. Some of the intermediate data points of the ΔG variation with *T* are shown in Table 17. The plot is shown in Fig. 37.

Table 17

Free energy change, ΔG as a function of temperature

Temperature, T (°K)	**Free energy change, ΔG (J/mol)**
600	49265.02
875	17805.63
1025	747.87
1031	0
1032	- 45.15
1075	- 4909.77

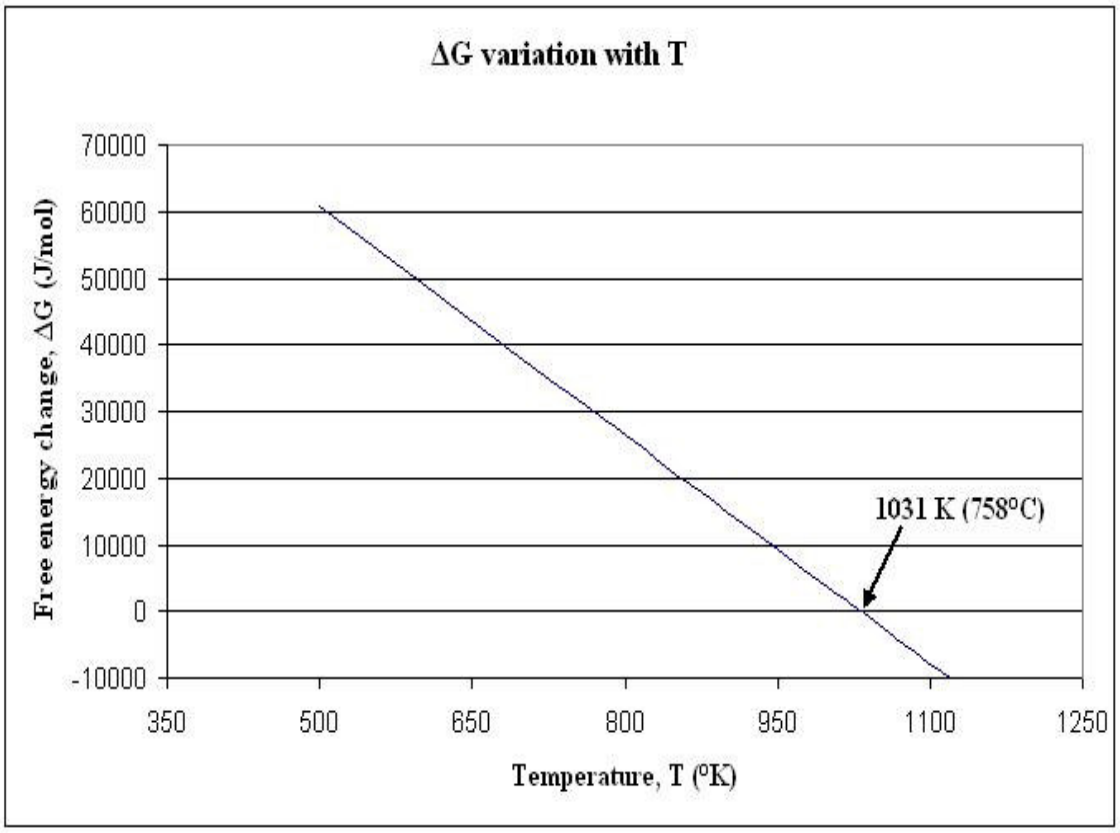

Fig. 37. Free energy change for the formation of Al_4C_3.

It is seen from the plot that ΔG decreases with temperature and it becomes zero at approximately 758°C (1031°K). This means that for the reaction to proceed, the temperature should be at least 758°C. Below this temperature, the thermodynamic driving force, dictated by ΔG, is positive which would prevent the interface reaction (1). FEA results were used to find the temperature distribution in the weld pool.

Region A of the weld pool was not considered for comparison, since concentration of the SiC particles was negligible in this region as explained earlier in Fig. 29. Region B was considered in the microstructures of the optimized specimens, where there was a higher occurrence of the SiC particulates. Higher instances of SiC

particles in region B of a specimen welded at the optimized level were found to start from a horizontal distance of 2.75 mm from the weld center line, at a height of 1.85 mm from the top surface of the weld. Fig. 38 shows the microstructure of this location in one of the specimens run at the optimized level. This location was used for the interface reaction analysis. It is clear that Al_4C_3 flakes, typically 15-30 μm long (Fig. 4), are not seen in this microstructure.

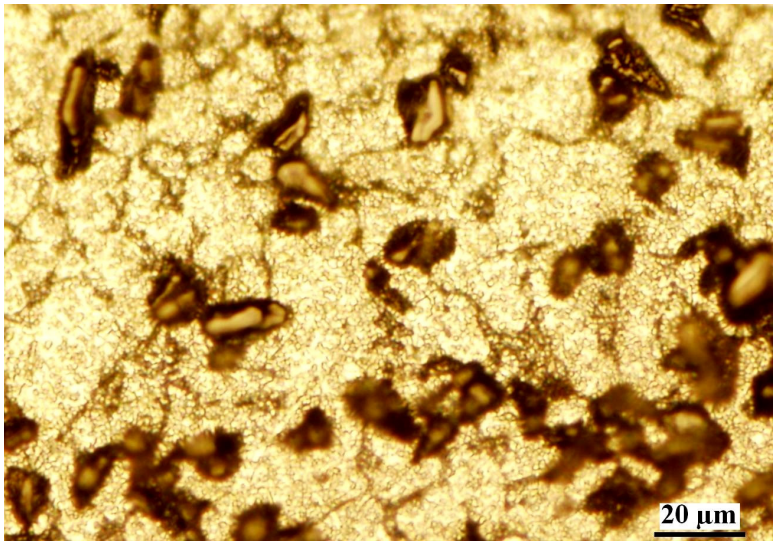

Fig. 38. Microstructure of a specimen in region B, welded at optimized conditions (85 A and 260 mm/min).

Temperatures at the same location were compared from the FEA results. It was found that the highest temperature reached in region B of the weld pool was approximately 776°C (1049°K) obtained by FEA, as explained later (Fig. 39). Though this temperature was higher than the critical temperature of 758°C, the time for which the pool was in this range of temperature was 5-7 seconds. Once the heat input from the welding torch was stopped, the temperature dropped suddenly, to 730°C (1003°K).

Though the interface reaction (1) might have just begun, the probability of it to continue was very less due to the sudden drop in the temperature of the weld pool.

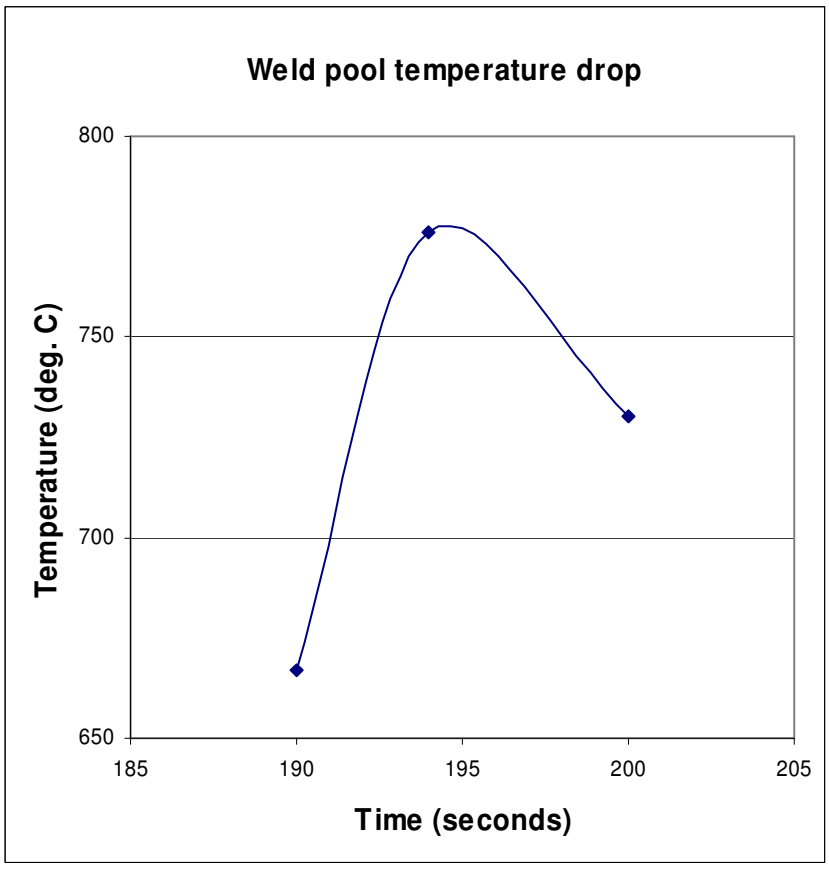

Fig. 39. FEA predicted weld pool temperature of region B in a specimen torch heated at 90 A and 14.5 V and welded at 85 A and 260 mm/min.

3. Microhardness test

The Vickers microhardness test on the optimized test was performed similar to that in the preliminary factorial tests. Fig. 40 shows the variation in the VHN across the

weld of a tensile tested specimen. It was seen that the weld center (region B) had an average of 72 VHN. As one traversed towards the end of the molten zone (region C), just before the HAZ, higher VHN in the range of 85-120 was found, with an average of 95. This region had higher dilution ratio and a microstructure equivalent to that of the base MMC; however, it had a finer microstructure than the base MMC due to comparatively faster cooling rates. In the HAZ, there was no significant loss of strength, with an average of 67 VHN. Similar hardness values were found in the specimen tested in bending, as shown in Fig. 41.

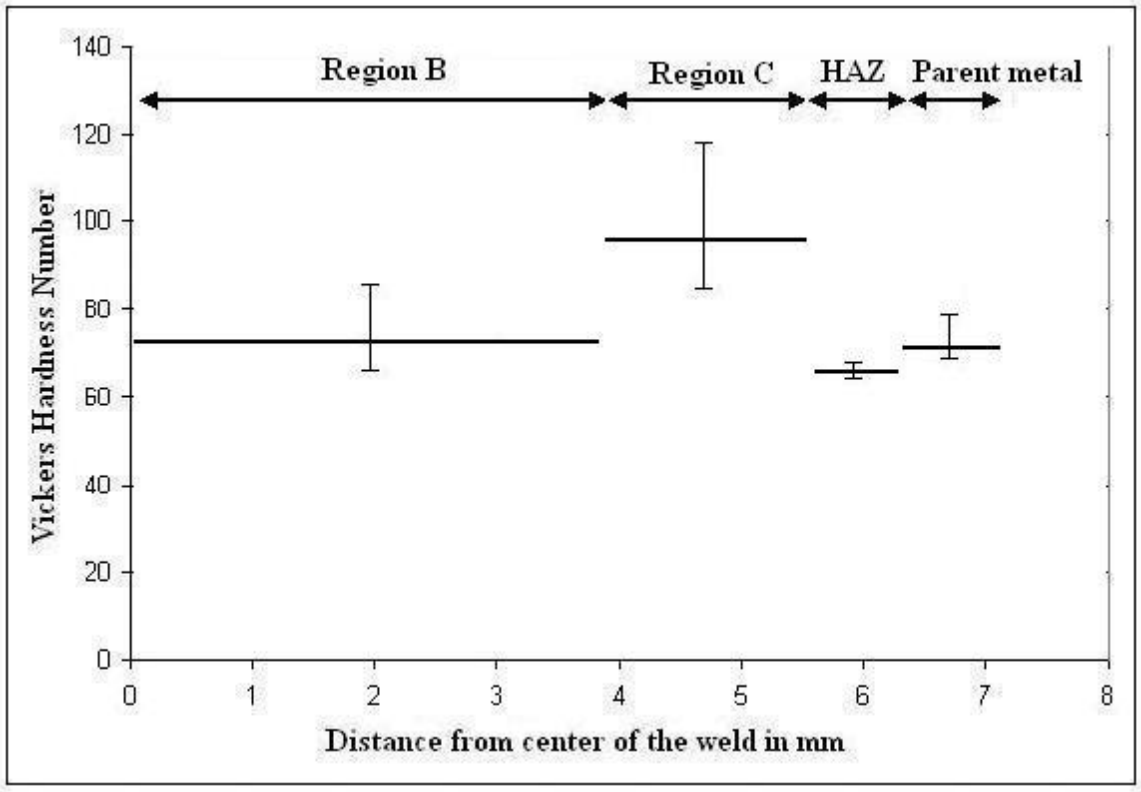

Fig. 40. VHN of the matrix across the weld of a tensile tested specimen, tested by 25 gm and for 10 seconds, welded at optimized conditions (85 A and 260 mm/min).

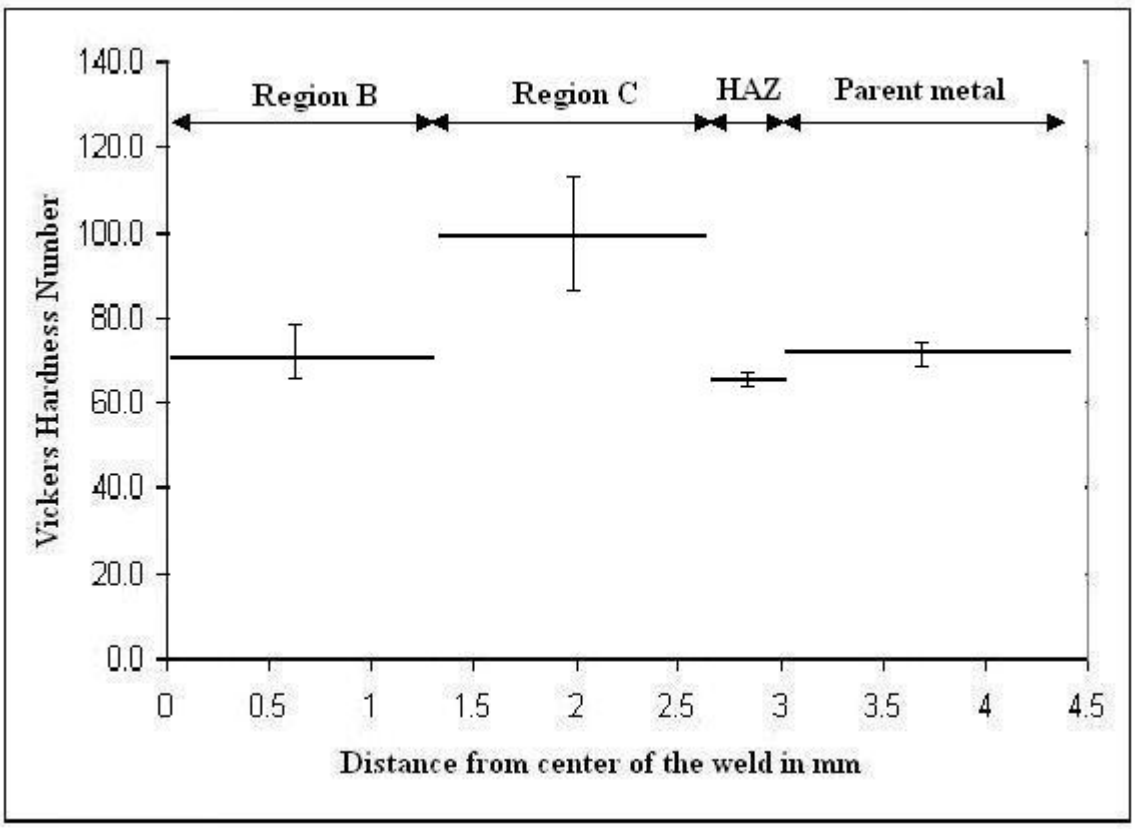

Fig. 41. VHN of the matrix across the weld of a bending tested specimen, tested by 25 gm and for 10 seconds, welded at optimized conditions (85 A and 260 mm/min).

V.5 Finite element analysis

V.5.1. Predicting preheat temperature

As mentioned earlier, the elements used in the FEA model were tetrahedral triangular elements. It was seen that this type of element generated better mesh in the model. Simulations also were run with other types of elements; however, producing unsatisfactory results, such as inability to capture intricacies along the weld joint. This

was primarily because of the triangular geometry of the weld joint. Further, the user-defined fine sized grid size helped to obtain exact temperature details along the joint. The mesh generated is shown in Fig. 42. In total, 18399 elements were generated in the mesh.

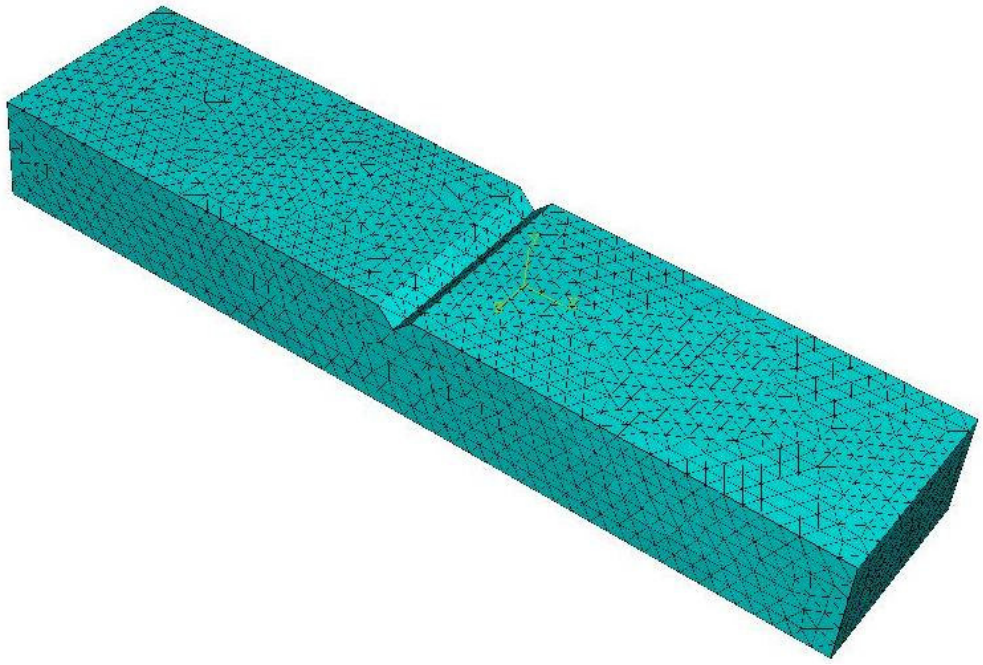

Fig. 42. Mesh generated for the preheat temperature FEA simulation.

The heat transfer efficiency was found to be one of the most critical input parameters in this analysis. Though the recommended value was known, in the range of 67-80%, it was very difficult to find the exact value to be used. Since it was applied on the tapered strips, it was found that a slight change in its values would impact the results significantly. Different values ranging from 67-80% were used and simulations were run until the peak temperatures obtained by the thermocouples were in close agreement with

the FEA results. Though it was a trial and error method, the assumptions were within the above specified range. It was finally found that a value of 70% provided satisfactory results and was utilized for further analysis.

The heat transfer coefficient had comparatively little effect on the output temperature values as compared to other input variables; however, since its literature range varied from 2-25 W/m^2 °K, some simulations were required to narrow its range. It was found that too high a value, of 22-25 W/m^2 °K, predicted lower temperature fields. An optimum value of 15 W/m^2 °K provided temperature fields which were in good agreement with the experimental values when coupled with the correct heat transfer efficiency.

The temperature values as recorded by the thermocouples were compared with those obtained by FEA and are plotted in Figs. 43, 44, and 45. It was seen that the FEA results were in good agreement with the experimental results. The assumptions thus made in the analysis were reasonable. Fig. 43 shows the experimental and FEA obtained temperature profiles at thermocouple location 1 (Fig. 20). It was seen that the actual thermocouple readings show peaks, which correspond to the sudden increase in the temperature when it is torch heated. Similarly, Figs. 44 and 45 show the temperature values at the other two locations**.**

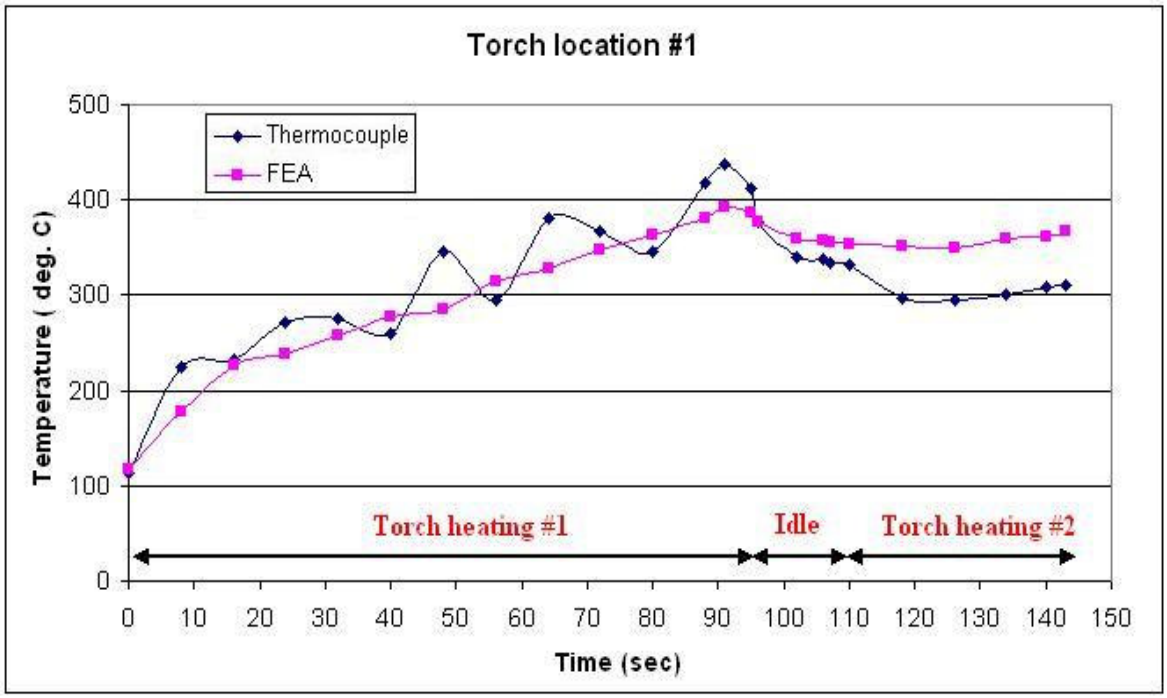

Fig. 43. Comparison of temperature profiles at torch location #1 (13 mm below the left preheat location #1) in a specimen torch heated at 90 A and 14.5 V.

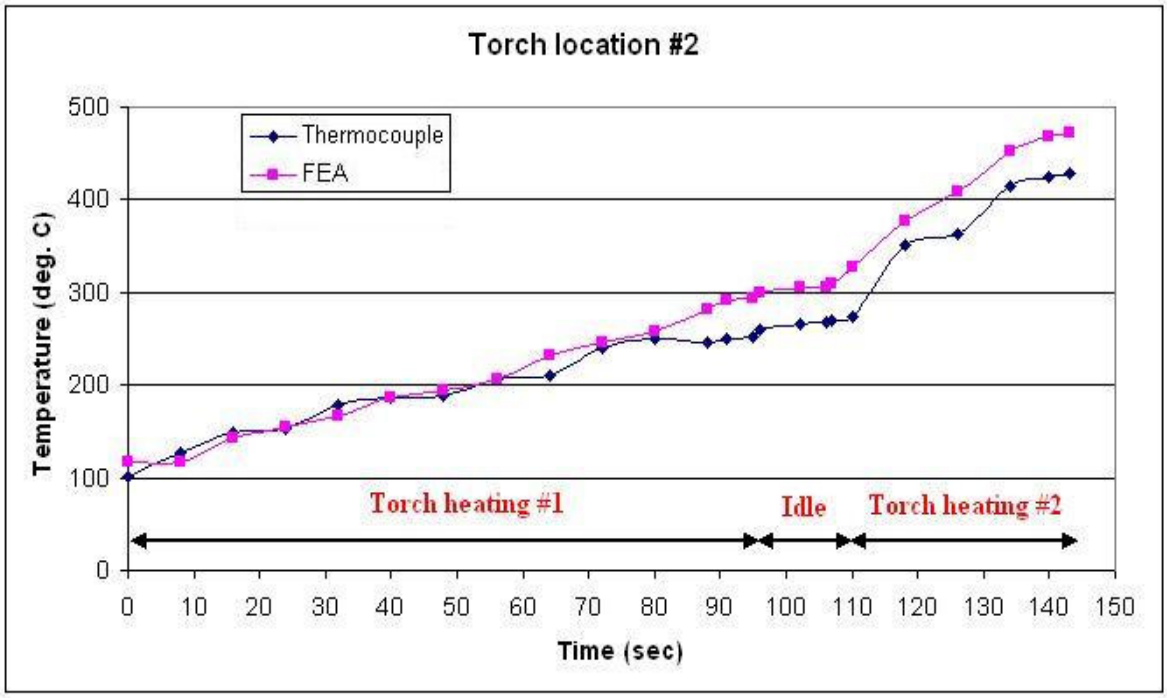

Fig. 44. Comparison of temperature profiles at torch location #2 (13 mm below the right preheat location #2) in a specimen torch heated at 90 A and 14.5 V.

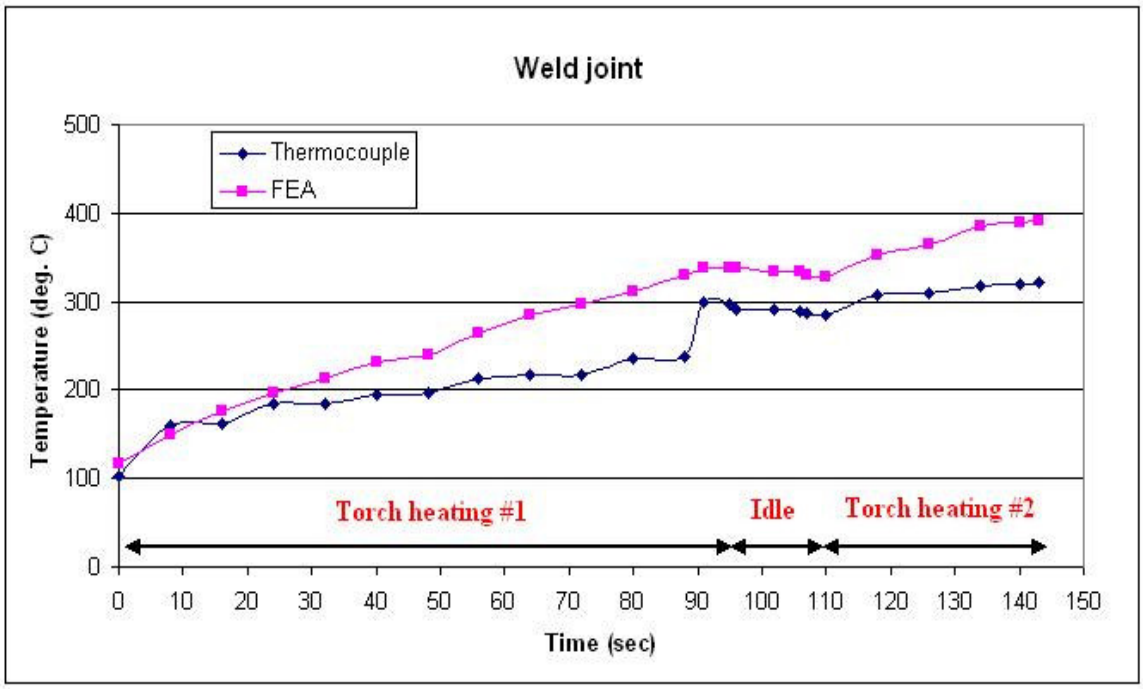

Fig. 45. Comparison of temperature profiles at the weld joint (10 mm below the top surface of the weld pool) in a specimen torch heated at 90 A and 14.5 V.

It was seen that the temperature field obtained from FEA, 10 mm below the top of the weld pool, was in the range of 375-395°C**,** as compared to 310-325°C as measured by the thermocouples. Further, the temperature range obtained from FEA just below the weld joint was also in the same range of 375-395°C. Since FEA predicted slightly higher range of temperatures, it was concluded that an approximate preheat temperature of 300-350°C was required to achieve good fusibility between the filler metal and the base metal. This preheat temperature further helps to weld the MMC at relatively low heat inputs.

V.5.2. Predicting the weld pool temperature field

The influence of the mesh size, element type, heat transfer coefficient, and heat transfer efficiency on the resulting temperature field was found to be the same as that in the FEA for predicting the preheat temperature, as expected. They were not varied and the simulation was continued from the previous simulation as explained in chapter IV. The FEA model generated is shown in Fig. 46. The mesh had a total of 9371 elements.

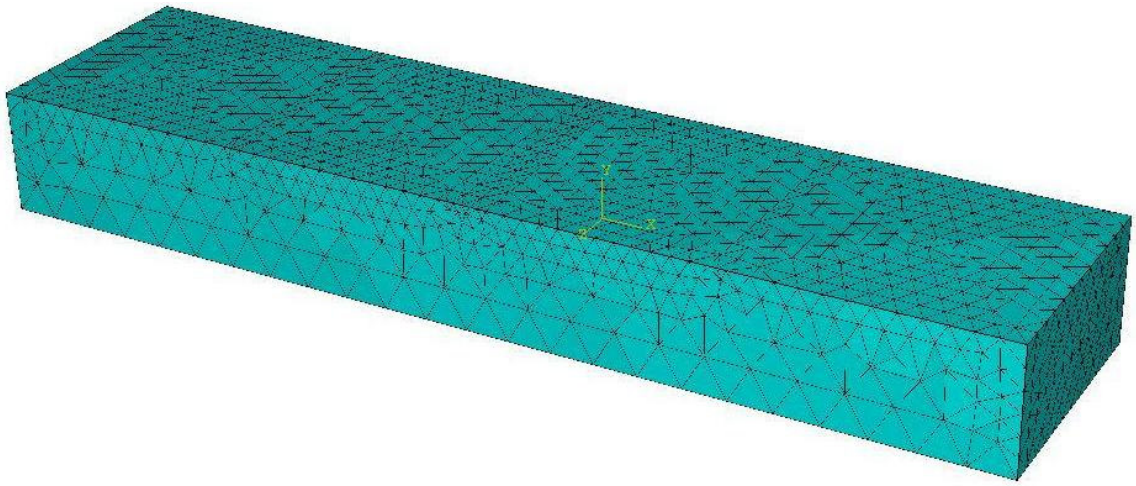

Fig. 46. Mesh generated for the weld pool temperature FEA simulation.

The FEA results were plotted at a node, which was at the same location as that of the SiC particles found in the microstructure, as explained earlier in this chapter (Fig. 38). Fig. 46 shows the temperature variation of a node in region B (Fig. 28) of the weld pool. Similar nature of the temperature field was found in this simulation as that of the previous simulation.

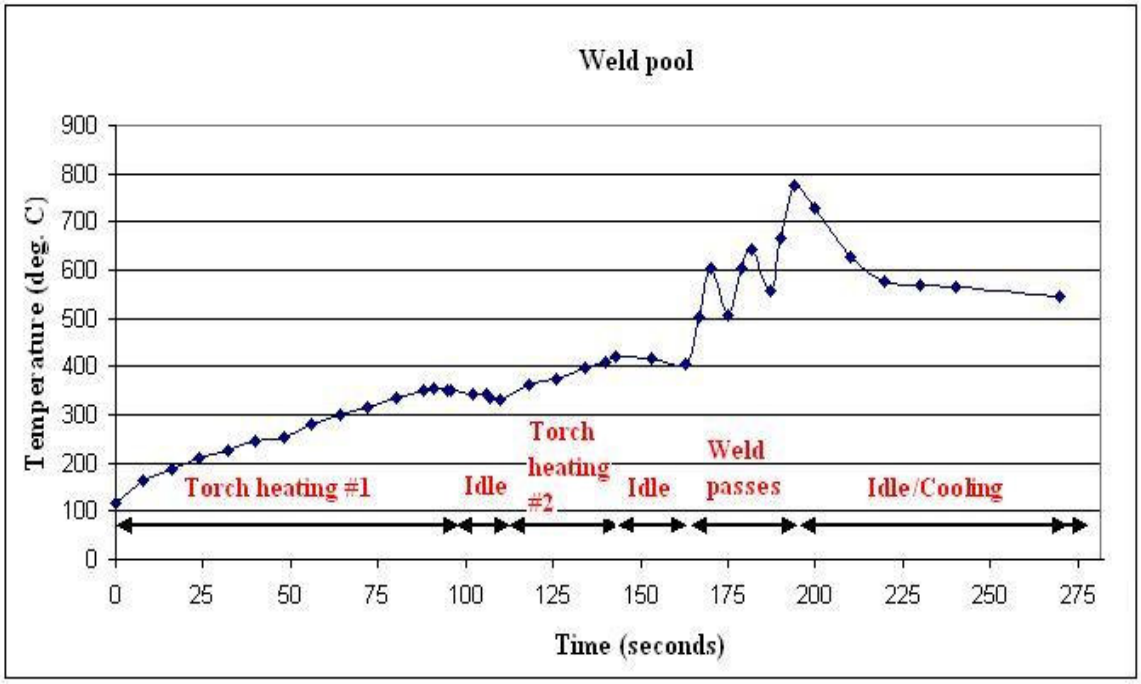

Fig. 47. FEA predicted weld pool temperature of region B (2.5 mm below the top surface) for a specimen torch heated at 90 A and 14.5 V and welded at optimized conditions of 85 A and 260 mm/min.

As explained earlier, it was seen that the maximum temperature reached at this node was approximately 776°C (1049°K) for a short amount of time of 5-7 seconds, after which the temperature drops suddenly, as seen in the above figure. This short resident time of the welding pool gave less reaction time for the interface reaction, making the weld joint Al_4C_3 free.

CHAPTER VI

CONCLUSIONS AND RECOMMENDATIONS

VI.1 Conclusions

The weldability of A359/SiC/10p MMCs was determined by systematically identifying the influence of the welding variables on their weld quality. Two level factorial experiments provided a good way of analyzing the effects of the welding variables. Selecting welding current and welding speed as the significant welding variables provided convincing results. The weld quality was measured with tensile and four point bending strengths, ductility variations, and microhardness across the weld. The weld microstructure was also analyzed with optical microscopy. Further, finite element analysis was used to complement the temperature results obtained during the experiments.

Preliminary factorial experiments, though unsuccessful in welding the MMCs, were very useful in determining the proper welding technique to weld this composite. It was found that local heating along the weld joint itself before welding led to the formation of thick layers of oxides along the joint. Also, since the composite had very limited fluidity, the pool was very rough and sluggish in appearance. It thus, was concluded that preheating to an appropriate range is inevitable during the welding of Al-SiCp MMCs.

Final factorial and the optimized experiments revealed that welding current and welding speed need to be properly controlled to keep the weld metal constituents in position. Ideally, in aluminum alloys, high heat input is favorable due to the high conductivity of aluminum; however, in case of Al-SiC MMCs, it was found and concluded that low and controlled heat inputs favored better quality welds, provided they were preheated. This led to a more uniform mixing of the base metal and the filler metal in the weld pool. This also helped to avoid the extremely reactive Al-SiC system from reacting with each other and preventing the formation of brittle aluminum carbide flakes.

To attain low heat inputs, low amperage and high welding speed should be used during GTAW of Al-SiC MMCs. The results obtained in this results could be obtained with 85 ± 5 A and 260 ± 20 mm/min.

Moreover, Al-Si filler metal, such as R-A356.0, should be used in their welding. Al-Si filler metal not only increased the fluidity of the viscous MMC molten pool, but also inhibited the reaction by increasing the Si content in the weld metal. Finally, it helped the easy movement of the SiC particles in the less viscous pool, towards the weld center. This led to high strength welds with increased ductility. The weld strengths were found to be approximately 85% of the parent MMC strength. The ductility of the welds was found to be approximately 150% higher than that of the parent MMC. The hardness values across the weld remained the same, except in the base metal rich region (Region C in the optimized tests).

Finite element analysis proved a very important research tool in determining the temperatures in the weld. Since it was not possible to attach thermocouples just below the weld fusion line, they were, however, used to find the temperatures at three different locations in the specimen. FEA was then helpful in comparing the results at these locations, and then was used to determine approximately the temperature just below the weld fusion line. From FEA, it was concluded that the temperature required just prior to welding should be 300-350°C along the weld line. Further, it was also concluded that the weld pool temperatures were below the critical temperature for the formation of Al_4C_3 flakes, helping to attain the desired weld integrity.

VI.2 Recommendations

To begin with, only three welding variables were selected for the factorial experimentation. In order to investigate the effects of other welding variables, further study is required. Though selected within recommended literature values and methods, some of the important welding factors such as arc length, gas flow rate, welding position, and bevel preparation method were treated as constant input factors in the

factorial experiments. A designed experiment, wherein the influence of these parameters could be investigated, would be ideal. Research work investigating the effect of these variables on this MMC would be very informative. This would result in many test runs, which was not possible in the present study due to the cost of the material and time involved in the process. With more replicates for each test condition, comprehensive knowledge about the welding phenomenon of Al-SiC MMCs can be achieved.

Butt joints of these MMCs may be performed in a manner similar to that done in this study. Preheating, a wide weld joint design, and low heat inputs are proposed to help the cause. It is recommended that oxides be cleaned mechanically before subsequent passes in case of multiple pass welds. Further, welding A359/SiC MMCs with different volume fractions of SiC particles may also be welded with the same filler metal and low heat density. It is proposed that welding of these MMCs with higher volume fraction of SiC particles should not pose any problems, since the interface reaction in these MMCs will accelerate faster and would be rich in Si content faster as compared to that in MMCs with low fractions of SiC particles.

The preheating technique used in this method was unique and not a standard preheating method. This method was applied, since this was the easiest and extremely beneficial in finding out the weldability of this composite material; however, its only drawback is that in practical applications, torch heating on either sides of the actual weld fusion line will not be feasible. Torch heating led to local melting of the material which ideally one would like to avoid. One of the alternative methods would be to oven heat the specimen to the desired temperature prior to welding. Another option will be to locally laser heat the weld joint in an inert atmosphere to avoid the formation of oxides. Electrical strip heaters attached around the location of the weld may also be a good alternative.

The testing methods used to evaluate the weld integrity were limited to destructive testing methods and optical microscopy. Non destructive testing such as radiographic inspection would be ideal to determine macroscopic defects in the interiors of the weld. Radiographs will help in analyzing the presence and nature of weld

discontinuities. Further, very limited information on the HAZ properties of the welded MMCs has been given in this study. A study to determine the HAZ properties of this MMC such as its impact strength, toughness, and grain size should be the undertaken in future.

Finite element analysis was restricted to finding the temperature distribution in the MMC when welded. Though the analysis was modeled with properties of the composite material as a whole, the composite material was characterized as a homogenous, isotropic material. This model did not take into consideration the variations that would arise otherwise. Further work recommended in this area could be analyzing the particle distribution effect and their properties on the weld temperatures. A micromechanics based model can be developed, wherein the model incorporates the actual orientation of the particle and its thermophysical properties can be taken into account. Previous work on developing a finite element micromodel for MMCs has been undertaken [27].

Friction stir welding (FSW) can be used for welding this MMC. This non-conventional type of welding developed recently has produced good results for various MMCs. It is a solid state process wherein the heat is produced due to the rubbing of the two faces. It uses a rotating probe which locally plasticizes the metal, reducing the heat input. Since no actual melting takes place, it can weld different combination of alloys without hot cracking. One of the other advantages is grain refinement due to high stirring and forging action. This process thus, is ideal for reactive systems like Al-SiC MMCs in theory. This welding process couldn't be used in this study since the entire equipment and the setup is very expensive.

REFERENCES

1) MBD Ellis, Int. Mater. Review 41 (1996) 41-58.
2) Alcan Inc., Metal matrix composites properties, http://mmcassess.tuwien.ac.at/data/prm/duralcan/aa6061_al2o3.htm, Accessed January 2004.
3) ASM 2 Metals Handbook, ASM International, Materials Park, OH, 1990.
4) K.A. Lucas, H. Clarke, Corrosion of aluminum-based metal matrix composites, John Wiley & Sons Inc., New York, 1993.
5) Kaiser Aluminum, Welding Kaiser aluminum, Kaiser Aluminum & Chemical Sales, Inc., Oakland, CA, 1978, pp. 8-1 – 8-21.
6) G. Mathers, The welding of aluminum and its alloys, Woodhead Publishing Limited, Cambridge, UK, 2002.
7) N. R. Mandal, Aluminum welding, ASM International, Materials Park, OH, 2002.
8) T. Luijendijk, Journal of Materials Processing Technology 103 (2000) 29-35.
9) A. H. Price, Improving the quality of welds for cryogenic applications, Ph.D. Dissertation, Texas A&M University, College Station, 1999.
10) B. Raj, C.V. Subramanian, T. Jayakumar, Non-destructive testing of welds, ASM International, Materials Park, OH, 2000.
11) W.H. Minnick, GTAW handbook, The Goodheart-Willcox Company, Inc., South Holland, IL, 1985.
12) ANSI/AWS B4.0-98 Standard methods for mechanical testing of welds, American Welding Society, Miami, FL, 1998.
13) M.M. Schwartz, Joining of composite matrix materials, ASM International, Materials Park, OH, 1994, pp. 89-90.
14) A. Urena, J.M. Gomez de Salazar, L. Gil, M.D. Escalera, J.L. Baldonedo, Journal of Microscopy 196 (1999) 124-136.

15) A. Urena, M.D. Escalera, L. Gil, Composites Science and Technology 60 (2000) 613-622.

16) M. Chen, C. Wu, J. Gao, Transactions of Nonferrous Metals Society of China 12 (5) (2002) 805-810.

17) S. Gopinathan, M.H. McCay, T.D. McCay, Processing of Advanced Materials 3 (1993) 213-224.

18) N.B. Dahotre, T.D. McCay, M H. McCay, Materials and Manufacturing Processes 9 (3) (1994) 447-466.

19) N. P. Hung, S. Jana, L. J. Yang, C. H. Heng, Proceedings, ASME, New York, AMD 208 MD 59 (1995b) 87-92.

20) N.P. Hung, N.L. Loh, V.C. Venkatesh, Machining of ceramics and composites, Marcel Dekker, New York, 1999, pp. 295-409**.**

21) Lincoln Electric, The procedure handbook of arc welding, The Lincoln Electric Company, Cleveland, OH, 1994.

22) CASTI Metals Data Book Series, CASTI metals blue book welding filler metals, ASM International, Materials Park, OH, 2002, pp. 252.

23) G. F. Vander Voort, Metallography principles and practice, ASM International, Materials Park, OH, 1999, pp. 610.

24) P. W. Fuerschbach, G. A. Knorovsky, Welding Journal 70 (1991) 287s-297s.

25) F. P. Incropera, D. P. DeWitt, Fundamentals of heat and mass transfer, John Wiley and Sons, New York, 1996.

26) W. D. Pilkey, Formulas for stress, strain, and structural matrices, John Wiley & Sons Inc., New York, 1994.

27) G. L. Heness, B. Ben-Nissan, L. H. Gan, Y-W. Mai, Computational Materials Science 13 (1999) 259-269.

VITA

MITUL ARVIND KOTHARI

175/8, Jawahar Nagar, Amizara Apartments,
Goregaon (West), Mumbai – 400062, India

EDUCATION

Texas A&M University, College Station, Texas 77843; M.S. in Mechanical Engineering, August 2005

Mumbai University, Mumbai 400062; B.S. in Mechanical Engineering, July 2002

PROFESSIONAL EXPERIENCE

Graduate Teaching Assistant, Department of Engineering Technology, Texas A&M University (January 2004 – May 2005); Assisted students with various manufacturing processes including welding and casting, and grading assignments.

Production Engineer, Tara Ultimo Pvt. Ltd., Mumbai, India (February 2003 – May 2003); Designed tool sets and fixtures for pneumatic rotating table heads, addressed daily operational issues, responsible for achieving daily targeted production from my unit.

Assistant Design Engineer, IndoGerman Pharma Equipments, Mumbai, India (August 2002 – December 2002); Involved in design phase of heat exchangers and fractional distillation plants, improved their stress distribution, and met structural safety margins.